

Precision Phenomenology at Colliders and Computational Methods

Gudrun Heinrich

KIT, Institute for Theoretical Physics (ITP)

Sommersemester 2021

version of May 28, 2021

Contents

1	Motivation: Collider Physics after the Higgs Discovery	4
1.1	Precision phenomenology	4
1.2	Perturbative expansions	7
2	A theoretical particle physicists' toolbox	14
2.1	Factorisation	14
2.2	Cross sections	17
2.2.1	Partonic cross section	17
2.2.2	Luminosity	18
2.2.3	Total hadronic cross section	19
2.2.4	Phase space integrals	19
2.3	Basics of QCD	24
2.3.1	Colour algebra	24
2.3.2	Experimental evidence for the existence of colour	31
2.3.3	QCD Lagrangian	36
2.3.4	QCD Feynman rules	42
3	Example: top quark production	44
3.1	Phenomenology	44
3.2	Top quark pair production	47
3.3	Higgs plus top quarks	48
3.4	New Physics effects (effective field theory)	49

4	Higher orders in perturbation theory	55
4.1	Running coupling and scale dependence	55
4.2	Loops and divergences	69
4.3	Dimensional regularisation	69
4.4	One-loop integrals	71
4.5	Cancellation of infrared singularities	79
4.6	Parton evolution	79
5	Example: Higgs production	79
5.1	Higgs boson production in gluon fusion	79
5.2	Higgs boson pair production	79
5.3	Asymptotic expansions	79

Literature

- G. Dissertori, I. Knowles, M. Schmelling,
Quantum Chromodynamics: High energy experiments and theory
International Series of Monographs on Physics No. 115,
Oxford University Press, Feb. 2003. Reprinted in 2005.
- R.K. Ellis, W.J. Stirling and B.R. Webber, *QCD and collider physics*,
Cambridge University Press, Camb. Monogr. Part. Phys. Nucl. Phys.
Cosmol. **8** (1996) 1.
- J. Campbell, J. Huston and F. Krauss,
*The Black Book of Quantum Chromodynamics: A Primer for the LHC
Era* Oxford University Press, December 2017.
- S. Dawson, C. Englert, T. Plehn,
Higgs Physics: It ain't over till it's over, <https://arxiv.org/abs/1808.01324>;
- L. J. Dixon, *A brief introduction to modern amplitude methods*,
<https://arxiv.org/abs/1310.5353>.
- G. Heinrich, *Collider Physics at the Precision Frontier*,
<https://arxiv.org/abs/2009.00516>.
- V. A. Smirnov, *Analytic tools for Feynman integrals*, Springer Tracts
Mod. Phys. **250** (2012) 1. doi:10.1007/978-3-642-34886-0.

1 Motivation: Collider Physics after the Higgs Discovery

1.1 Precision phenomenology

What is phenomenology (in physics)? According to Wikipedia:

In physics, phenomenology is the application of theoretical physics to experimental data by making quantitative predictions based upon known theories.

The big questions:

1. Are these “known theories” incomplete?
2. How to distinguish mis-modelling of the data from real “new physics” effects?
3. How can we profit maximally from the data to find out in which direction to extend our models?

To answer questions 1) and 2), high precision of the theory predictions as well as reliable uncertainty estimates are mandatory. To address question 3), it is necessary to identify observables which are sensitive to particular extensions of the Standard Model and which can be measured and calculated with small uncertainties.

Of course, if new particles are produced directly, they can appear as clear resonances in the data, such that precision is not necessary for the discovery. This was the case for the Higgs boson discovery, see Fig. 1. However, in the current situation of particle physics, it looks like new particles (if existent) are too heavy to be produced directly at present colliders, or too weakly interacting to have been noticed so far. This is again where precision comes into play.

It is often said that the Standard Model (SM) is very well tested, however “very well” often means order 10% deviations from the prediction are acceptable. With the High-Luminosity-LHC however, the precision of important SM measurements will be at the few percent level, and if the theory predictions cannot keep up with this, it would be a waste of data and experimental resources.

What is the status today?

The particle content of the SM is shown in Fig. 2.

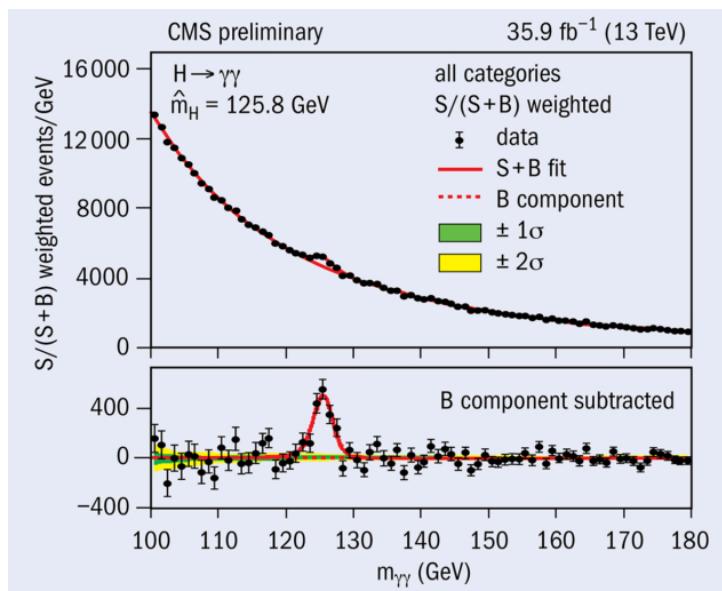


Figure 1: The Higgs boson resonance for $H \rightarrow \gamma\gamma$. *Source: CERN Courier*

Fig. 3 shows the current status of measurements of SM cross sections. Measurements of couplings of the Higgs boson are shown in Fig. 4.

Higgs bosons can be produced in various ways, the main production channels at the LHC are shown in Fig. 5.

Persistent deviations from the SM prediction in the decay of B-mesons have recently been confirmed by the LHCb collaboration [2]. A slide from the talk at the Moriond 2021 conference by M. Alguero is shown in Fig. 6.

The results, which imply a violation of *lepton flavour universality*, could be explained by the existence of so-called “Leptoquarks”, mediating a direct interaction between quarks and leptons, see Fig. 7, or by the existence of a Z' -boson, see Fig. 8.

If there are additional bosons mediating lepton flavour violating interactions, they are probably too heavy to be produced directly at the LHC.

Another very recent hint towards physics beyond the SM is the new measurement of the anomalous magnetic moment of the muon at Fermilab [4]. The measured value is 4.2 standard deviations away from the (perturbatively calculated) SM prediction, see Fig. 9.

For a recent theory review see Ref. [5].

The situation today may be similar to the one before the discovery of the

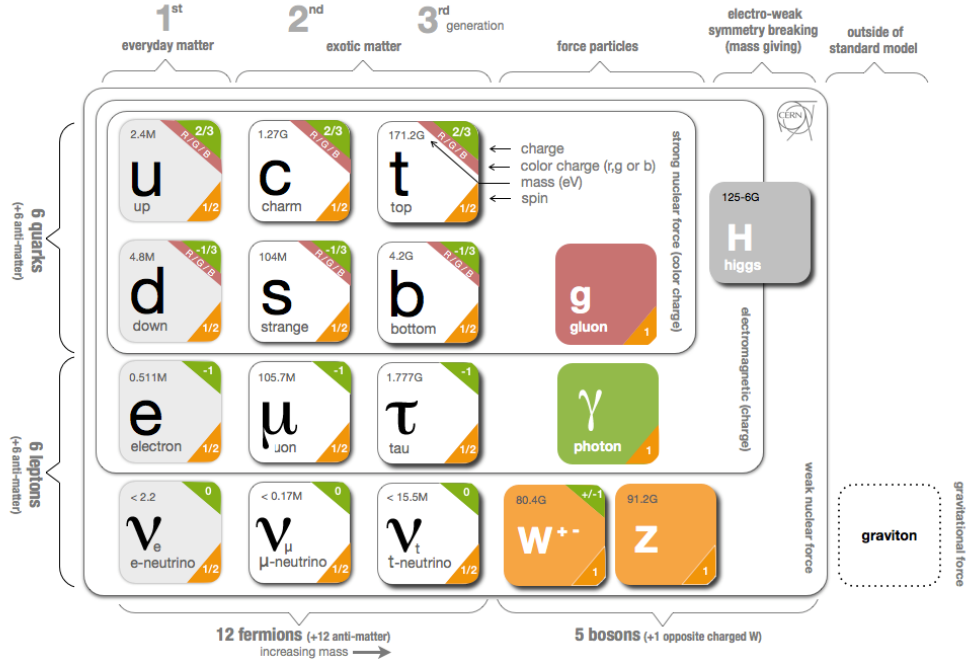


Figure 2: The particles of the Standard Model. *Source: CERN*

W^- and Z -bosons (1983). Fig. 10 shows the energy region around the Z -resonance for the process $e^+e^- \rightarrow$ hadrons. For energies below the W^+W^- production threshold the amplitude is composed of a diagram with virtual photon exchange, $M^{(\gamma^*)} \sim 1/q^2$ and a diagram with Z -boson exchange, $M^{(Z)} \sim 1/(q^2 - M_Z^2) - iM_Z\Gamma_Z$. For $q^2 \ll M_Z^2$ the virtual photon exchange diagram dominates and the cross section falls off like $1/s$. This is shown in Fig. 11. At collider energies that do not exceed $\sqrt{s} \sim 40$ GeV, no sign of deviation from pure QED can be detected. An interesting region is the one between $40 \text{ GeV} \lesssim \sqrt{s} \lesssim 60 \text{ GeV}$, where the energy is not sufficient to see a resonance, but deviations from the QED prediction can be identified if the prediction is precise enough. Similar arguments hold for the on-set of W -boson pair production. Today we may be in a similar situation. As higher order corrections also tend to enhance the corresponding cross sections, it is obvious that a reliable estimate of their size is essential before claims of “new

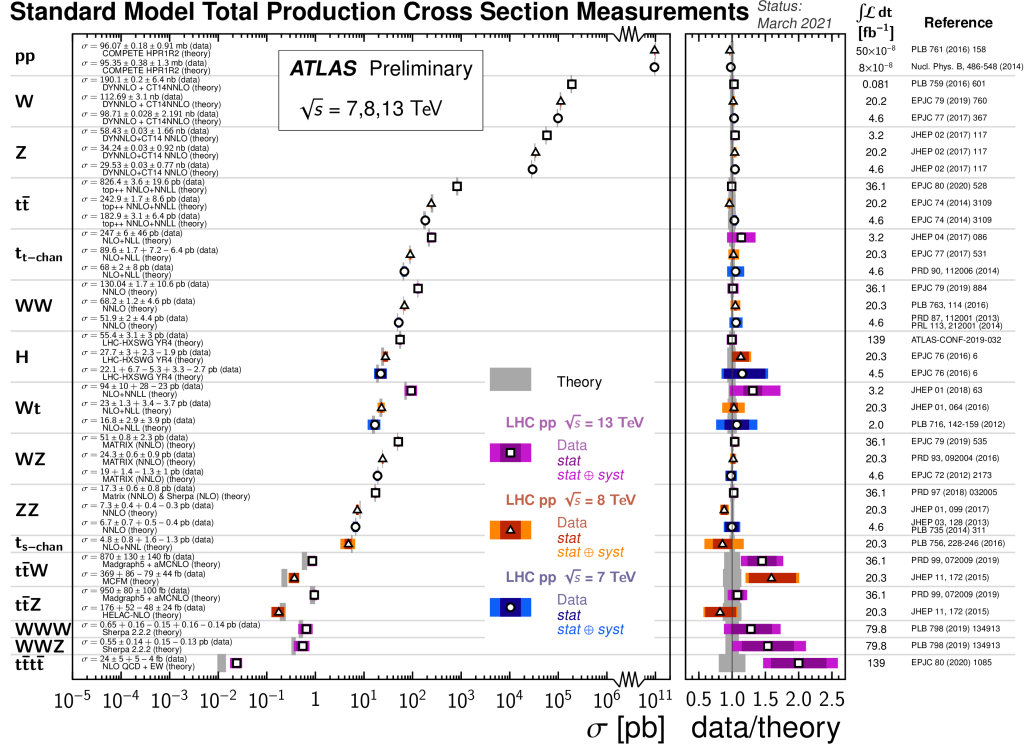


Figure 3: Summary of SM cross section measurements. *Source: Ref. [1]*

physics signals” can be made in the absence of direct detection of resonances.

1.2 Perturbative expansions

In perturbative quantum field theory, precision is closely tied to the calculation of higher orders in an expansion in the strong coupling α_s or the electroweak coupling α . For example, the expansion of a cross section can be expanded in a power series in α_s as

$$\sigma = \sigma^{LO} + \alpha_s \sigma^{NLO} + \alpha_s^2 \sigma^{NNLO} + \dots, \quad (1)$$

where LO means “leading order”, NLO “next-to-leading order”, $NNLO$ “next-next-to-leading order”, etc. The leading order cross section σ^{LO} itself may contain nonzero powers of α_s or α already, however the above power series indicates the QCD-corrections, which, at NLO, can be classified into

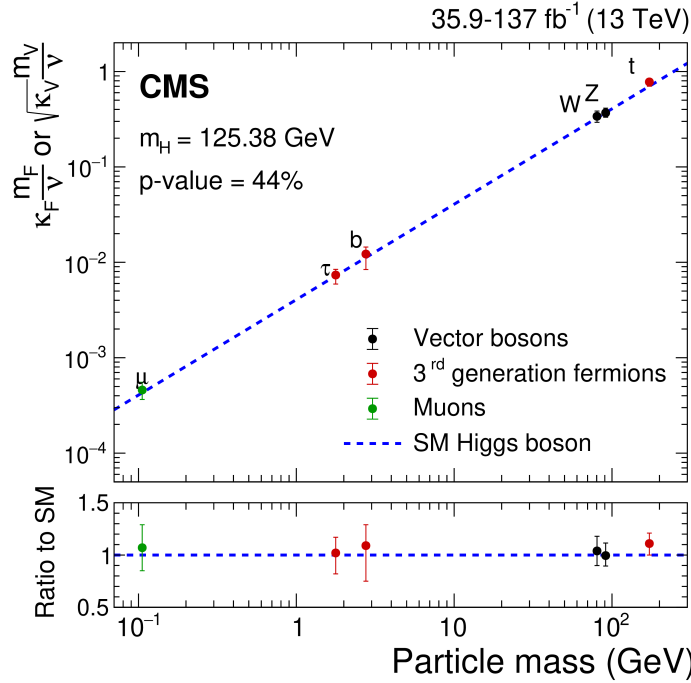


Figure 4: Comparison of Higgs coupling measurements to the SM expectation. *Source: <https://twiki.cern.ch/twiki/bin/view/CMSPublic>*

real and *virtual* corrections, where the real corrections implies the radiation of extra QCD particles (gluons or quarks), while the virtual corrections contain loops of extra virtual particles with QCD couplings. We will go through explicit examples in this lecture. Beyond NLO, combinations of virtual and real corrections will also occur. How important NNLO corrections can be to describe the data is shown in Fig. 12.

As the value of the strong coupling at the energy scale of the Z-boson mass is $\alpha_s(M_Z) \simeq 0.118$, while the electroweak (EW) coupling, $\alpha(M_Z)$, amounts to about $1/128$, QCD corrections of the same power in the coupling are in general larger than EW corrections. Rule of thumb:

NLO QCD: $\mathcal{O}(10\%)$ corrections, NNLO QCD: few % corrections, NLO EW: few % corrections. However, there are important cases where this rule does not apply, for example

- Higgs production in gluon fusion: NLO QCD corrections $\mathcal{O}(100\%)$;
- kinematic regions where EW corrections are enhanced due to large

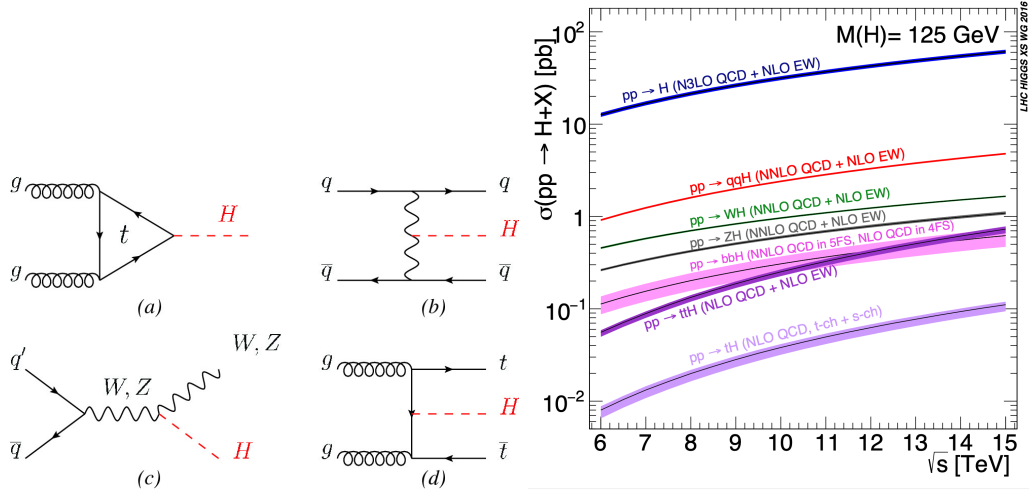


Figure 5: Illustrative Feynman diagrams for the main Higgs boson production channels (left) and corresponding cross sections (right). Source: <https://twiki.cern.ch/twiki/bin/view/LHCPhysics/LHCHWG>

logarithms of the form $\ln\left(\frac{M_W^2}{\hat{s}}\right)$, where $\hat{s} \gg M_W^2$, for example weak boson production;

- kinematic regions dominated by soft and/or collinear radiation (also called infrared radiation), where large logarithms of the form $\ln\left(\frac{M^2}{p_\perp^2}\right)$ occur, for example in the transverse momentum spectrum of a particle or particle pair at low transverse momentum p_\perp . As the infrared behaviour of QED and QCD is universal, i.e. process independent, such logarithmic terms can be predicted and the perturbative series can be re-organised. This is called *resummation*;
- mixed QCD \otimes EW corrections also need to be considered when percent level precision is aimed at.

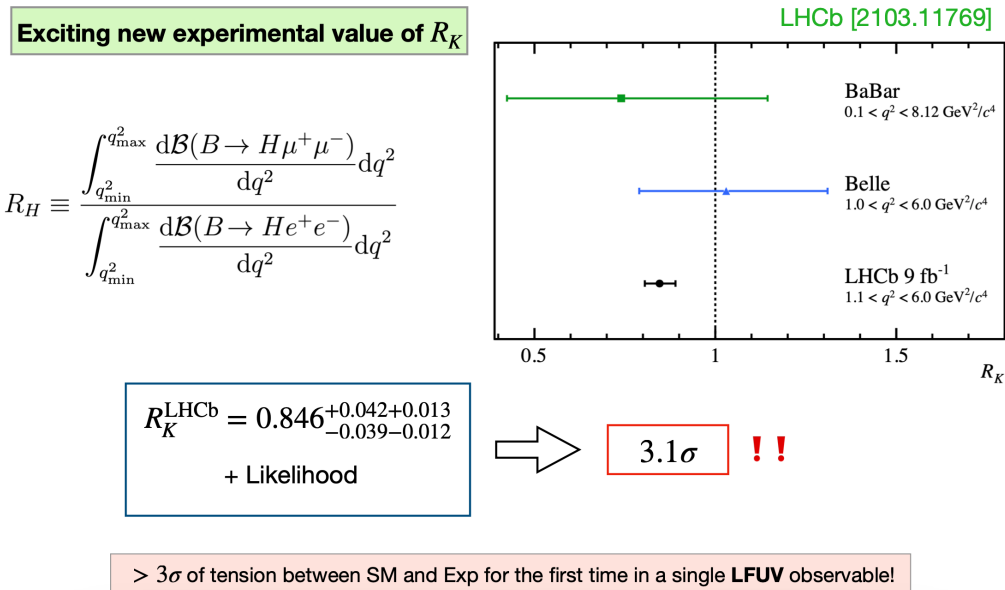


Figure 6: Deviations from the SM in B-decays, talk by M. Alvaro, Moriond 2021, based on Ref. [2].

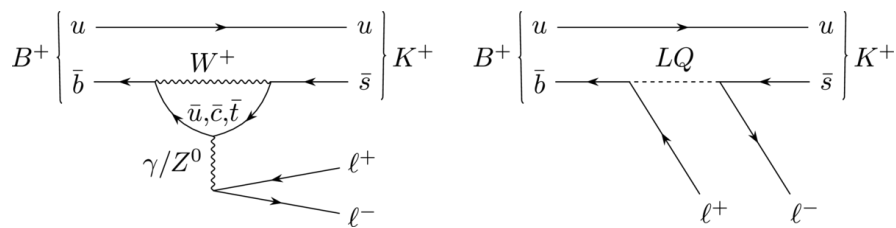


Figure 7: SM diagram and leptoquark-exchange diagram. Figure from Ref. [2].

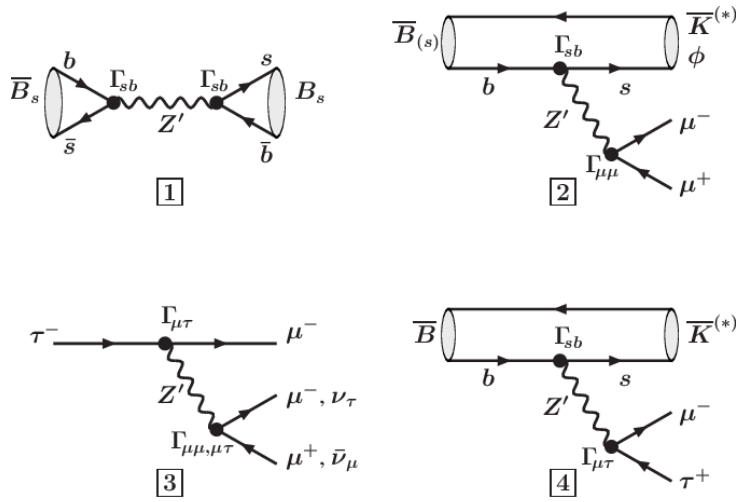


Figure 8: Z' -exchange diagram. Figure from Ref. [3].

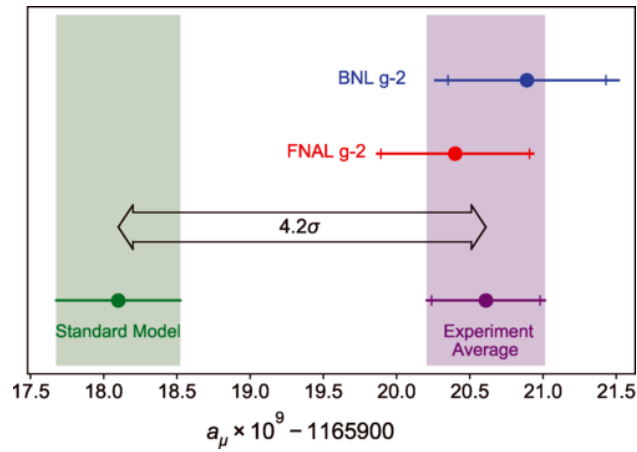


Figure 9: Measured values of the muon anomalous magnetic moment compared to the SM prediction. Figure from Ref. [4].

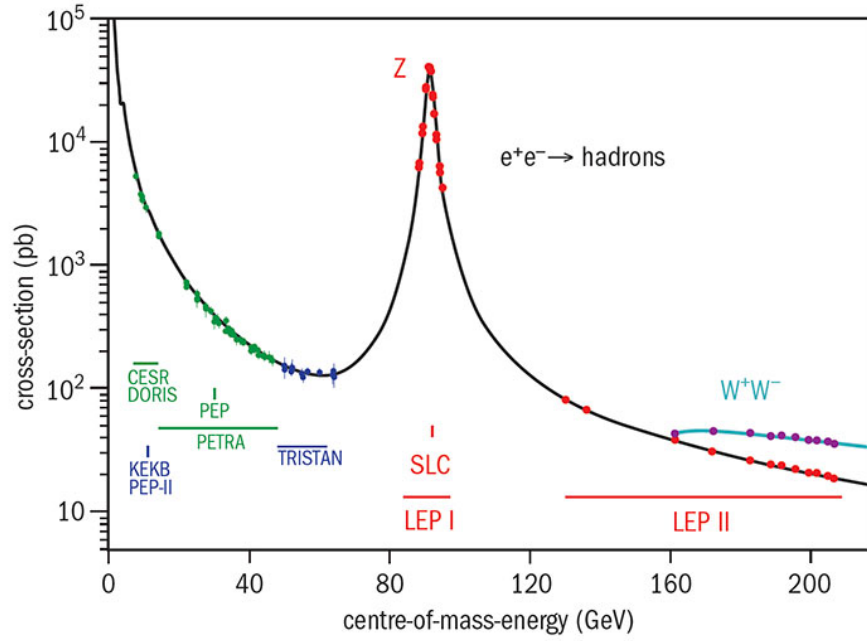


Figure 10: Z -resonance. Figure from Ref. [6].

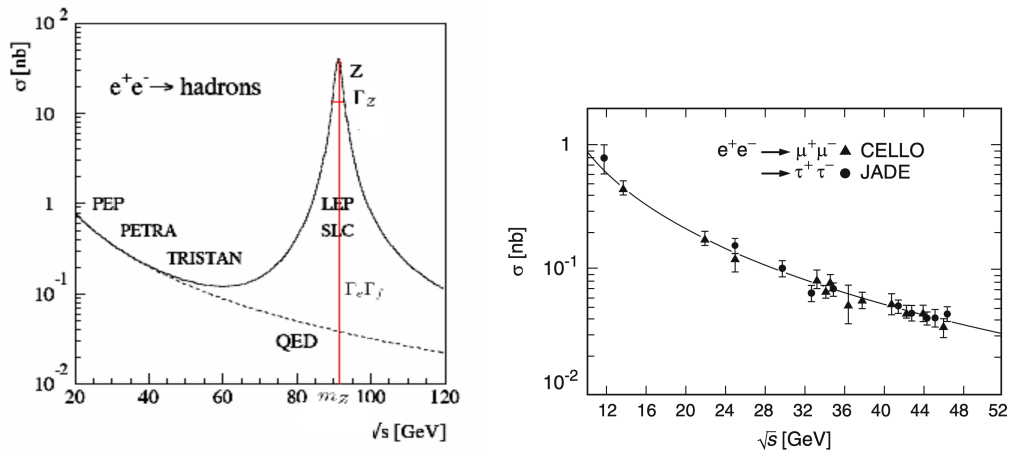
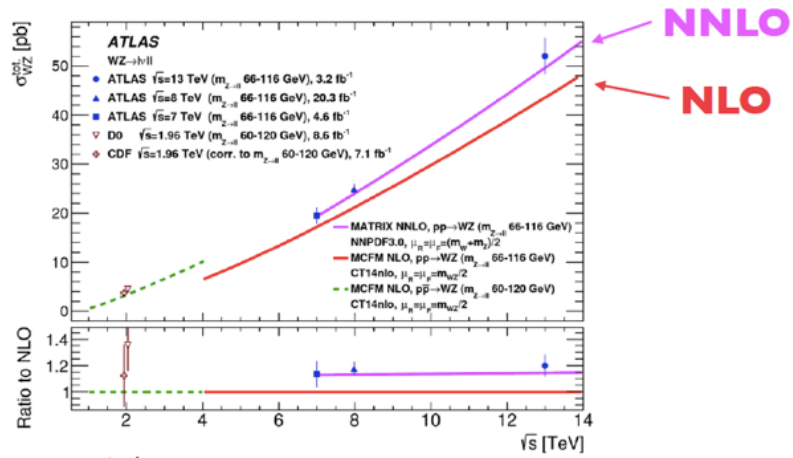


Figure 11: Z -resonance and cross section from QED only (left) and measurements confirming the QED prediction (right).



M. Wiesemann et al.

Figure 12: WZ measurement compared to NLO and NNLO predictions.

2 A theoretical particle physicists' toolbox

2.1 Factorisation

A typical event at a hadron collider like the LHC is quite complicated, as sketched in Fig. 13. As the proton is a bound state of quarks and gluons, non-perturbative aspects play a role in the initial state, and of course also in the final state, because quarks and gluons hadronize. Only the red blobs and the yellow parton branchings can be described perturbatively. It is quite non-trivial that we can describe such complex interactions with high accuracy. The fact that we can separate the event into a part that is calculable in perturbation theory, the *hard scattering cross section* (also called partonic cross section), and a non-perturbative part is called *factorisation*. Factorisation would not be possible without *asymptotic freedom*, the fact that the strong coupling $\alpha_s(Q^2)$ decreases as the energy scale Q^2 increases.

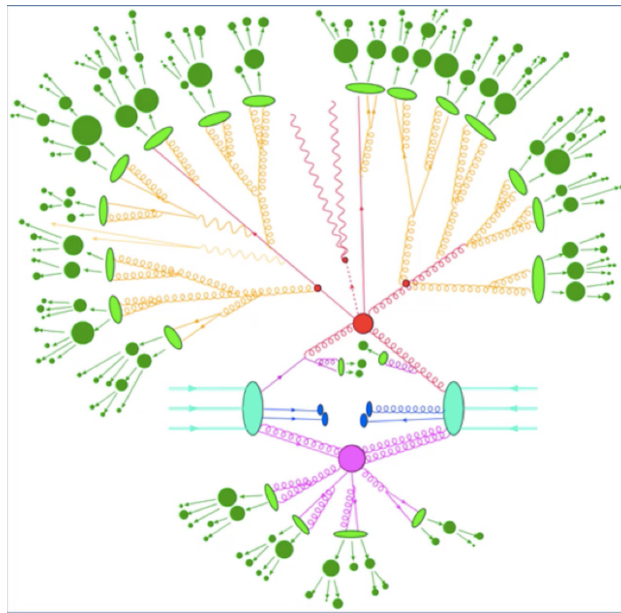


Figure 13: Schematic picture of a LHC event. *Figure by G. Luisoni*

The basic formula for factorisation at hadron colliders is the convolution of parton distribution functions (PDFs) with the partonic cross section. For example, the differential cross section for a process like the production

of a Higgs boson, $p_a + p_b \rightarrow H + X$, has the form

$$d\sigma_{pp \rightarrow H+X} = \sum_{i,j} \int_0^1 dx_1 f_{i/p_a}(x_1, \alpha_s, \mu_f) \int_0^1 dx_2 f_{j/p_b}(x_2, \alpha_s, \mu_f) \times d\hat{\sigma}_{ij \rightarrow H+X}(x_1, x_2, \alpha_s(\mu_r), \mu_r, \mu_f) + \mathcal{O}\left(\frac{\Lambda}{Q}\right)^p. \quad (2)$$

Factorisation, shown in Fig. 14, holds up the the so-called *power corrections* of order $\left(\frac{\Lambda}{Q}\right)^p$ (the power p is process-dependent, but always positive, $\Lambda \simeq 250$ MeV is the scale where non-perturbative effects start to dominate the behaviour of the strong coupling). Therefore, the larger the energy scale Q^2 of the hard process, the smaller the power corrections.

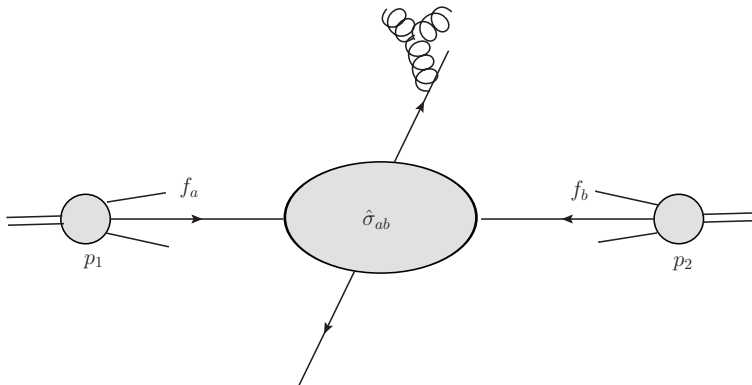


Figure 14: Schematic picture of factorisation in hadron-hadron collisions.

Strictly speaking, the above factorisation is called “collinear factorisation”, because it assumes that the partons which are coming from the hadrons a and b have a momentum which is collinear to the parent hadron momentum. There is also the so-called “transverse momentum dependent (TMD)” factorisation, which takes into account that the partons inside the proton can have a transverse momentum relative to the beam axis. This requires transverse momentum dependent PDFs, see e.g. Ref. [7] for a review. The TMD effects can become sizeable for example in Drell-Yan production ($pp \rightarrow V \rightarrow l^+l^-$) at very low transverse momenta of the produced vector boson, or in semi-inclusive DIS (deep-inelastic scattering).

We will discuss the PDFs as well as asymptotic freedom in more detail later, here we want to stress that without factorisation, it would not be possible

to produce the high precision predictions as we have them today within a strongly interacting theory, i.e. QCD.

As the PDFs themselves cannot be calculated from first principles, but need to be fitted from data, their contribution to the uncertainty budget increases in relative size the more higher orders in perturbation theory are available for the partonic cross section. The current situation for the case of Higgs production in gluon fusion is shown in Fig. 15. Predictions based on different PDFs for ratios of Drell-Yan measurements are shown in Fig. 16.

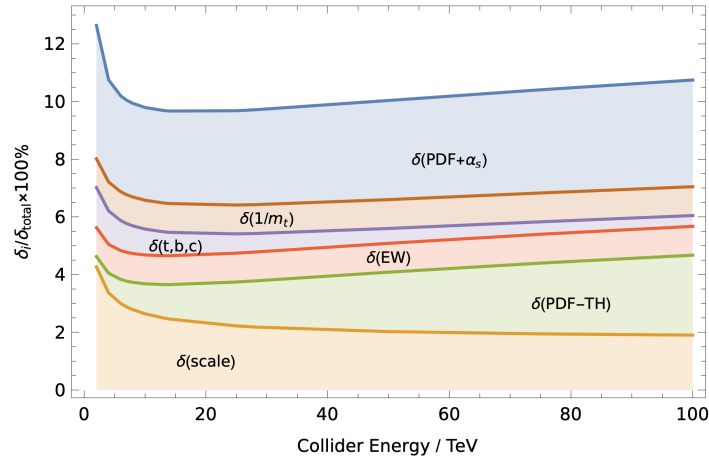


Figure 15: Contributions to the total uncertainty for Higgs production in gluon fusion. Figure from Ref. [8].

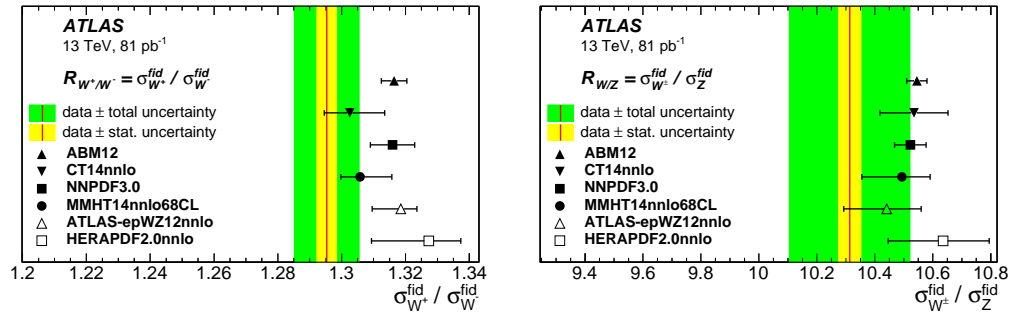


Figure 16: Comparison of predictions to recent measurements of fiducial W - and Z -production cross sections. Figures from Ref. [9].

2.2 Cross sections

2.2.1 Partonic cross section

The partonic cross section $\hat{\sigma}_{ij}$ in eq. (2) can be calculated order by order in perturbation theory. It contains the modulus of the scattering or decay matrix element, $|\mathcal{M}|^2$, which encodes the fundamental interactions derived from the Lagrangian.

For a reaction $p_i + p_j \rightarrow p_1 + \dots + p_n$, the reaction rate is calculated according to Fermi's golden rule based on the transition matrix element $|\mathcal{M}|^2$. We have

$$d\hat{\sigma} = \frac{J}{\text{flux}} \cdot |\mathcal{M}|^2 \cdot d\Phi_n, \quad (3)$$

where

$$\text{flux} = 4\sqrt{(p_i \cdot p_j)^2 - m_i^2 m_j^2}.$$

Assuming massless incoming particles and calculating in the centre-of-mass frame of $p_i + p_j$ we therefore have $\text{flux} = 4p_i \cdot p_j = 2\hat{s}$, with $\hat{s} = (p_i + p_j)^2$. The quantity $J = 1/j!$ is a statistical factor to be included for each group of j identical particles in the final state. The phase space volume spanned by the final state particles is denoted by $d\Phi_n$, it will be considered in more detail in section 2.2.4.

For a decay process $Q \rightarrow p_1 + \dots + p_n$ we have

$$d\Gamma = \frac{J}{2\sqrt{Q^2}} \cdot |\mathcal{M}|^2 \cdot d\Phi_n. \quad (4)$$

If the spins of the final state particles are not measured, we sum over all possible polarisations in the final state. Colour in the final state cannot be measured, so we also have to sum over all colours in the final state. Further, we average over colours and polarisations in the initial state. The matrix element is then given by

$$|\mathcal{M}|^2 \rightarrow \overline{|\mathcal{M}|^2} = \prod_{\text{initial}} \frac{1}{N_{\text{pol}} N_{\text{col}}} \sum_{\text{pol, col}} |\mathcal{M}|^2 \quad (5)$$

quarks: $N_{\text{col}} = N_c, N_{\text{pol}} = 2$

gluons: $N_{\text{col}} = N_c^2 - 1,$

$$N_{\text{pol}} = \begin{cases} D - 2 & \text{in conventional dimensional regularisation} \\ 2 & \text{other schemes (HV, DRED)} \end{cases}.$$

The expression for the gluon polarisations already anticipates that we will calculate in $D = 4 - 2\epsilon$ dimensions rather than four space-time dimensions later, in order to regulate the singularities that appear at higher orders in perturbation theory.

The expression $\overline{\sum |\mathcal{M}|^2}$ is often just written as $|\overline{\mathcal{M}}|^2$.

2.2.2 Luminosity

If we look at the scattering in a very general way and scatter particles of type a with particle density n_a on a fixed target with particle density n_b and depth d , see Fig. 17. If F is the area of the beam and v_a the velocity of the beam particles, the flux is given by

$$\text{flux} = n_a v_a = \frac{\dot{N}_a}{F}, \quad (6)$$

where \dot{N}_a is the number of particles per time unit [s]. The number of target particles situated within the beam area is $N_b = n_b F d$, and $L = \text{flux} \cdot N_b$ is called the *luminosity*. The *reaction rate* is defined as

$$R = L \cdot \sigma_r,$$

where σ_r is the *cross section* for reaction r .

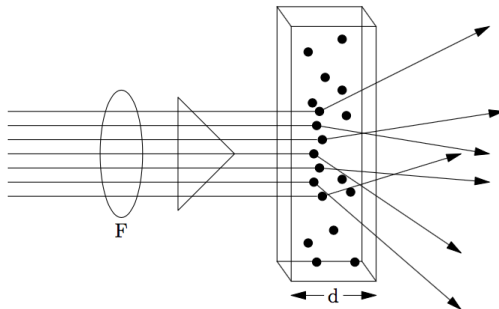


Figure 17: Scattering on a fixed target with depth d .

Differential cross sections can be defined for example in terms of the angular distributions of the scattered particles. The reaction rate per volume element $d\Omega$ is given by

$$\frac{dR(\theta, \phi)}{d\Omega} = L \frac{d\sigma(\theta, \phi)}{d\Omega} \quad \text{such that} \quad \sigma = \int_0^{2\pi} d\phi \int_{-1}^1 d \cos \theta \frac{d\sigma(\theta, \phi)}{d\Omega}. \quad (7)$$

For a circular collider with two bunches crossing each other rather than hitting a fixed target, we have

$$L = f \cdot n \cdot \frac{N_a N_b}{F} , \quad (8)$$

where f is the bunch frequency, n is the number of bunches, N_a and N_b are the numbers of particles per bunch, and F is the bunch crossing area. Cross sections are usually given in units of ‘barn’, where 1 barn $\simeq 10^{-24}\text{cm}^2$. Using $L = 10^{34}\text{cm}^{-2}\text{s}^{-1}$ for the LHC luminosity, for cross sections of $\mathcal{O}(100)$ pb (1 picobarn = 10^{-12} barn) we have a rate of 1 event per second. As an example, for top quark pair production at 14 TeV we have $\sigma_{t\bar{t}} \simeq 1000$ pb which leads to ~ 10 events per second.

2.2.3 Total hadronic cross section

The hadronic cross section σ at a centre-of-mass energy s is often written in terms of the partonic cross section and a luminosity function

$$\mathcal{L}_{ij}(x_1, x_2, \mu_f) = f_{i/p_a}(x_1, \mu_f) f_{j/p_b}(x_2, \mu_f) , \quad (9)$$

such that

$$\sigma(s) = \int_{\hat{s}_{min}}^s d\hat{s} \int_0^1 dx_1 \int_0^1 dx_2 \delta(\hat{s} - x_1 x_2 s) \sum_{i,j} \mathcal{L}_{ij}(x_1, x_2, \mu_f) \int d\hat{\sigma}_{ij}(x_1, x_2, \mu_r, \mu_f) , \quad (10)$$

where $f_i(x, \mu_f)$ is the parton distribution function (PDF) of a parton with momentum fraction x and flavour i (including gluons) and μ_f is the factorisation scale.

2.2.4 Phase space integrals

Phase space integrals in D dimensions

The general formula for a phase space $d\Phi_n$ with n particles in the final state in D space-time dimensions is given by

$$\begin{aligned} d\Phi_n &= \prod_{j=1}^n \left[\frac{d^D p_j}{(2\pi)^{D-1}} \delta^+(p_j^2 - m_j^2) \right] (2\pi)^D \delta\left(Q - \sum_{j=1}^n p_j\right) \\ &= (2\pi)^{n-D(n-1)} \prod_{j=1}^n \left[d^D p_j \delta(p_j^2 - m_j^2) \Theta(E_j) \right] \delta\left(Q - \sum_{i=1}^n p_i\right) , \quad (11) \end{aligned}$$

where Q can be a single particle momentum or $Q = q_1 + q_2$ in the $2 \rightarrow n$ scattering case. We use

$$d^D p_j \delta(p_j^2 - m_j^2) \Theta(E_j) = dE_j d^{D-1} \vec{p}_j \delta(E_j^2 - \vec{p}_j^2 - m_j^2) \Theta(E_j) = \frac{1}{2E_j} d^{D-1} \vec{p}_j \Big|_{E_j = \sqrt{\vec{p}_j^2 + m_j^2}}$$

for $j = 1, \dots, n$ to arrive at

$$d\Phi_n = (2\pi)^{n-D(n-1)} \prod_{j=1}^n \frac{d^{D-1} \vec{p}_j}{2E_j} \delta\left(E_{\text{cm}} - \sum_{i=1}^n E_i\right) \delta^{(D-1)}\left(\sum_{i=1}^n \vec{p}_i\right), \quad (12)$$

We will use the last δ -function to eliminate \vec{p}_n . We further use

$$d^{D-1} \vec{p} f(|\vec{p}|) = d\Omega_{D-2} d|\vec{p}| |\vec{p}|^{D-2} f(|\vec{p}|), \quad (13)$$

where $d\Omega_{D-2}$ is the surface element in $D-2$ dimensions, $V(D-1)$ is the volume of a unit sphere in $D-1$ dimensions.

$$\begin{aligned} \int_{S_{D-2}} d\Omega_{D-2} &= V(D-1) = \frac{2\pi^{\frac{D-1}{2}}}{\Gamma(\frac{D-1}{2})}, \\ \int d\Omega_{D-2} &= \int d\Omega_{D-3} \int_0^\pi d\theta (\sin \theta)^{D-3} = \int_0^\pi d\theta_1 (\sin \theta_1)^{D-3} \int_0^\pi d\theta_2 (\sin \theta_2)^{D-4} \dots \int_0^{2\pi} d\phi \end{aligned}$$

to obtain

$$d\Phi_n = (2\pi)^{n-D(n-1)} 2^{-n} \prod_{j=1}^{n-1} \left[d\Omega_{D-2}^{(j)} \frac{d|\vec{p}_j|}{E_j} |\vec{p}_j|^{D-2} \right] \frac{1}{E_n} \delta\left(E_{\text{cm}} - \sum_{i=1}^n E_i\right), \quad (14)$$

with $E_j = \sqrt{\vec{p}_j^2 + m_j^2}$. Note that in the massless case $E_j = |\vec{p}_j|$, such that the above formula simplifies.

Phase space for $2 \rightarrow 2$ scattering with massive final state particles

We consider the process $p_1 + p_2 \rightarrow p_3 + p_4$ with $p_3^2 = m_3^2, p_4^2 = m_4^2$. Using a momentum parametrisation in the centre-of-mass frame, we have

$$\begin{aligned} p_1 &= \frac{\sqrt{\hat{s}}}{2} (1, 0, 0, 1) \\ p_2 &= \frac{\sqrt{\hat{s}}}{2} (1, 0, 0, -1) \\ p_3 &= (E_3, 0, p_f \sin \theta, p_f \cos \theta) \\ p_4 &= (E_4, 0, -p_f \sin \theta, -p_f \cos \theta) \end{aligned}$$

where

$$p_f = \frac{\sqrt{\lambda(\hat{s}, m_3^2, m_4^2)}}{2\sqrt{\hat{s}}}; E_i = \sqrt{m_i^2 + p_f^2} \quad (15)$$

and $\lambda(\hat{s}, m_3^2, m_4^2) = (\hat{s} - (m_3 + m_4)^2)(\hat{s} - (m_3 - m_4)^2)$ is the Källén function,

$$\lambda(x, y, z) = x^2 + y^2 + z^2 - 2(xy + xz + yz).$$

Defining $m_+ = m_3 + m_4, m_- = m_3 - m_4$ and $\beta^2 = \left(1 - \frac{m_+^2}{s}\right) \left(1 - \frac{m_-^2}{s}\right)$, we have $\lambda(\hat{s}, m_3^2, m_4^2) = \hat{s}^2 \beta^2$ and we can write

$$\begin{aligned} \hat{t} &= (p_2 - p_3)^2 = \frac{1}{2} (m_3^2 + m_4^2) - \frac{\hat{s}}{2} (1 + \beta \cos \theta), \\ \hat{u} &= (p_1 - p_3)^2 = \frac{1}{2} (m_3^2 + m_4^2) - \frac{\hat{s}}{2} (1 - \beta \cos \theta). \end{aligned} \quad (16)$$

As p_f must be real we have $\hat{s}_{min} = (m_3 + m_4)^2$.

From Eq. (14) the $2 \rightarrow 2$ phase space in the centre-of-mass frame is given by

$$\int d\hat{\Phi}_{2 \rightarrow 2} = \frac{1}{(2\pi)^{D-2}} \int d\Omega_{D-2} d|\vec{p}_3| \frac{|\vec{p}_3|^{D-2}}{2E_3 2E_4} \delta(E_{\text{cm}} - E_3 - E_4). \quad (17)$$

The δ -constraint can be evaluated to eliminate $|\vec{p}_3| \equiv p$:

$$\begin{aligned} \delta(E_{\text{cm}} - E_3 - E_4) &\equiv \delta(f(p)) = \delta \left(E_{\text{cm}} - \sqrt{p^2 + m_3^2} - \sqrt{p^2 + m_4^2} \right) \\ &= \left(\frac{p}{E_3} + \frac{p}{E_4} \right)^{-1} \delta(p - p_f), \end{aligned} \quad (18)$$

where p_f is the solution of $f(p) = 0$, leading to $p_f = \frac{1}{2E_{\text{cm}}} \sqrt{\lambda(E_{\text{cm}}^2, m_3^2, m_4^2)}$ as already given above. Inserting this into Eq. (17) leads to

$$\begin{aligned} \int d\hat{\Phi}_{2 \rightarrow 2} &= \frac{1}{(2\pi)^{D-2}} \frac{1}{4} \int d\Omega_{D-2} \frac{p_f^{D-3}}{E_{\text{cm}}}, \\ d\Omega_{D-2} &= \int_0^{2\pi} d\phi \int_0^\pi (\sin \theta)^{D-3} d\theta. \end{aligned} \quad (19)$$

So in 4 dimensions with ϕ integrated out and covariant notation:

$$\int d\hat{\Phi}_{2 \rightarrow 2} = \frac{1}{16\pi} \frac{\sqrt{\lambda}}{\hat{s}} \int_{-1}^1 d \cos \theta. \quad (20)$$

Combined with the integration over the momentum fractions x_i from the convolution with the PDFs, we have

$$\int d\Phi_{2 \rightarrow 2} = \frac{1}{16\pi} \int_0^1 dx_1 \int_0^1 dx_2 \int_{\hat{s}_{\min}}^s d\hat{s} \delta(\hat{s} - x_1 x_2 s) \frac{\sqrt{\lambda}}{\hat{s}} \int_{-1}^1 d \cos \theta.$$

Note: The 3-particle phase space $d\Phi_3(Q \rightarrow p_3 + p_4 + p_5)$ can conveniently be written as the 2-particle phase space for the production of a pseudo-particle with momentum $P_{34} = p_3 + p_4$, $P_{34}^2 = s_{34}$, combined with the phase space for the subsequent splitting $P_{34} \rightarrow p_3 + p_4$,

$$d\Phi_3(Q \rightarrow p_3 + p_4 + p_5) = \frac{ds_{34}}{2\pi} d\Phi_2(Q \rightarrow P_{34} + p_5) d\Phi_2(P_{34} \rightarrow p_3 + p_4). \quad (21)$$

This procedure can be iterated, viewing the n -particle phase space as a sequential decay chain. However this is not always the most efficient phase space for each topology of Feynman diagrams (and their interferences). Often done in practice: *multi-channelling*: write $|\mathcal{M}|^2$ as

$$|\mathcal{M}|^2 = \frac{|\sum_i \mathcal{M}_i|^2}{\sum_i |\mathcal{M}_i|^2} \sum_i |\mathcal{M}_i|^2 \quad (22)$$

and optimize the phase space for each $|\mathcal{M}_i|^2$, using the ratio as a weight.

Phase space for $1 \rightarrow 3$ processes with massless particles

For $n = 3$ in Eq. (11) one can choose a coordinate frame such that

$$\begin{aligned}
Q &= (E, \vec{0}^{(D-1)}) \\
p_1 &= E_1 (1, \vec{0}^{(D-2)}, 1) \\
p_2 &= E_2 (1, \vec{0}^{(D-3)}, \sin \theta, \cos \theta) \\
p_3 &= Q - p_2 - p_1,
\end{aligned} \tag{23}$$

leading to

$$\begin{aligned}
d\Phi_{1 \rightarrow 3} &= \frac{1}{4} (2\pi)^{3-2D} dE_1 dE_2 d\theta_1 (E_1 E_2 \sin \theta)^{D-3} d\Omega_{D-2} d\Omega_{D-3} \\
&\quad \Theta(E_1) \Theta(E_2) \Theta(E - E_1 - E_2) \delta((Q - p_1 - p_2)^2).
\end{aligned} \tag{24}$$

A parametrisation in terms of the Mandelstam variables $s_{ij} = 2p_i \cdot p_j$ can often also be useful, therefore we make the transformation $E_1, E_2, \theta \rightarrow s_{12}, s_{23}, s_{13}$. To work with dimensionless variables we define $y_1 = s_{12}/Q^2$, $y_2 = s_{13}/Q^2$, $y_3 = s_{23}/Q^2$ which leads to

$$\begin{aligned}
d\Phi_{1 \rightarrow 3} &= (2\pi)^{3-2D} 2^{-1-D} (Q^2)^{D-3} d\Omega_{D-2} d\Omega_{D-3} dy_1 dy_2 dy_3 \\
&\quad (y_1 y_2 y_3)^{D/2-2} \Theta(y_1) \Theta(y_2) \Theta(y_3) \delta(1 - y_1 - y_2 - y_3).
\end{aligned} \tag{25}$$

The latter can be derived easily if we relate the Jacobian $|\det J|$ to the determinant of the Gram matrix $G_{ij} = 2p_i \cdot p_j$, where G_{ij} can as well be formed from Q, p_1, p_2 rather than p_1, p_2, p_3 . Using

$$\begin{aligned}
s_{12} &= 2E_1 E_2 (1 - \cos \theta) \\
s_{13} &= 2E_1 (E - E_2 (1 - \cos \theta)) = E (E - 2E_2) \\
s_{23} &= 2E_2 (E - E_1 (1 - \cos \theta)) = E (E - 2E_1)
\end{aligned} \tag{26}$$

the Jacobian for the transformation is

$$|\det J| = \left| \det \left(\frac{\partial(s_{12}, s_{13}, s_{23})}{\partial(E_1, E_2, \theta)} \right) \right| = 8E^2 E_1 E_2 \sin \theta. \tag{27}$$

The Gram matrix is given by

$$G = \begin{pmatrix} 0 & s_{12} & s_{13} \\ s_{12} & 0 & s_{23} \\ s_{13} & s_{23} & 0 \end{pmatrix} \tag{28}$$

such that

$$\det G = 2s_{12}s_{13}s_{23} = 8E^2 E_1^2 E_2^2 \sin^2 \theta \quad (29)$$

and therefore

$$\det J = 2E\sqrt{2 \det G} = 4E \sqrt{s_{12}s_{13}s_{23}}. \quad (30)$$

This leads to

$$\begin{aligned} \int d\theta_1 dE_1 dE_2 [E_1 E_2 \sin \theta]^{D-3} &= \int d\theta_1 dE_1 dE_2 \left[\frac{\det J}{8E^2} \right]^{D-3} \\ &= \int ds_{12} ds_{13} ds_{23} (8E^2)^{3-D} (\det J)^{D-4} \\ &= E^{2-D} 2^{1-D} \int ds_{12} ds_{13} ds_{23} \left(\frac{\det G}{2} \right)^{\frac{D-4}{2}}. \end{aligned}$$

Combining everything and rescaling the Mandelstam invariants with Q^2 leads to Eq. (25) above. This procedure can be generalised to $1 \rightarrow n$ phase spaces.

2.3 Basics of QCD

2.3.1 Colour algebra

The strong interactions can be described as an $SU(3)$ local gauge theory, where the ‘‘charges’’ are denoted as *colour*, therefore the name ‘‘Quantum Chromodynamics’’ (QCD). QCD is embedded in the Standard Model with underlying gauge group structure $SU(3) \times SU(2)_L \times U(1)_Y$. Often the number of colours is denoted generically by N_c and the colour algebra in QCD calculations is done for a generic $SU(N_c)$ gauge group (we believe that in nature $N_c = 3$, but the concept is more general). Using a generic N_c has many advantages, for example it allows to divide the amplitudes into simpler building blocks according to their colour structure.

The group $SU(N_c)$ is an example of so-called *Lie groups* (Sophus Lie, 1842-1899), which will be discussed below. For QED the underlying group is $U(1)$. As we will see, the group structure of $SU(N_c)$ implies that gluons interact with themselves (while photons do not).

Groups

A group G is a set of elements g with a multiplication $G \times G \rightarrow G$ which satisfies:

- there is a unit element e with $g \circ e = e \circ g = g$,
- for each g an inverse exists g^{-1} with $g \circ g^{-1} = g^{-1} \circ g = e$,
- associativity $g_1 \circ (g_2 \circ g_3) = (g_1 \circ g_2) \circ g_3$.

For *Abelian* groups: $g_1 \circ g_2 = g_2 \circ g_1$. (Niels Henrik Abel, 1802-1829).

We will deal with compact Lie groups, which are groups whose elements depend analytically on a finite number of continuous parameters. The group $SU(N)$ is a Lie group whose representations are unitary matrices with determinant one.

$$SU(N)\text{representations} : \{U \in \mathbb{C}^{N \times N} | UU^\dagger = 1 \wedge \det U = 1\}. \quad (31)$$

Each $U \in SU(N)$ can be written as

$$U = \exp \{i \theta_a T^a\}, \quad \theta_a \in \mathbb{R}, \quad (32)$$

from $UU^\dagger = 1$ it follows that $T^a = (T^a)^\dagger$, from $\det U = 1$ (with $\det U = e^{\text{Tr}(\ln U)}$) follows $\text{Tr}(T^a) = 0$.

Other examples of Lie groups are the orthogonal groups $SO(N)$, e.g. the rotation group $SO(3)$, the symplectic groups $Sp(N)$ and the special groups G_2, F_4, E_6, E_7, E_8 .

Representations

A *representation* of a group is a mapping of the group elements onto matrices, where the group multiplication laws translate to matrix multiplication (preserving the group multiplication laws), i.e. linear algebra can be used.

Any group element which can be obtained from the identity by continuous changes in the parameters can be written as $\exp(iT^a\theta^a)$ where θ^a are real parameters and T^a are linearly independent hermitian operators. The set of all linear combinations $T^a\theta^a$ is a vector space and the T^a form a basis in that space. Therefore they are also called the *generators* of the group.

For the generators T^a , the commutation relation

$$[T^a, T^b] = i f^{abc} T^c \quad (33)$$

holds, independent of the representation, defining an algebra associated with the group. The f^{abc} are called *structure constants*. For Abelian groups the structure constants are zero.

Further, the generators satisfy the *Jacobi identity*

$$[T^a, [T^b, T^c]] + [T^b, [T^c, T^a]] + [T^c, [T^a, T^b]] = 0, \quad (34)$$

which translates into a relation between structure constants.

The generators are normalised such that

$$\text{Trace}(T^a T^b) = T_R \delta^{ab}. \quad (35)$$

Usually one chooses $T_R = 1/2$ for the fundamental representation, which we will also do.

While the (totally antisymmetric) structure constants are given in terms of generators by

$$f^{abc} = -2i \text{Trace}(T^a [T^b, T^c]), \quad (36)$$

we can also define totally symmetric constants by

$$d^{abc} = 2 \text{Trace}(T^a \{T^b, T^c\}). \quad (37)$$

For us, two representations of $SU(N)$ will be important:

1. the *fundamental representation*: the generators are $N \times N$ matrices,
2. the *adjoint representation*: the generators of this representation are $(N^2 - 1) \times (N^2 - 1)$ -matrices, i.e. the indices run over the same range as the number of generators (the number of generators is called the *dimension* of the group). So in the adjoint representation the dimension of the vector space in which the representation matrices act equals the dimension of the group. Therefore the generators in the adjoint representation can be expressed in terms of structure constants:

$$T_{bc}^a = (F^a)_{bc} =: -i f^{abc}, \quad a, b, c = 1 \dots N^2 - 1. \quad (38)$$

The generators of $SU(3)$ in the fundamental representation are usually defined as $t_{ij}^a = \lambda_{ij}^a/2$, where the λ_{ij}^a are also called *Gell-Mann* matrices. They are traceless and hermitian and can be considered as the $SU(3)$ analogues of the Pauli-matrices for $SU(2)$ (in fact, the first three λ^i generate an $SU(2)$ subgroup of $SU(3)$).

$$\lambda^1 = \begin{pmatrix} 0 & 1 & 0 \\ 1 & 0 & 0 \\ 0 & 0 & 0 \end{pmatrix}, \quad \lambda^2 = \begin{pmatrix} 0 & -i & 0 \\ i & 0 & 0 \\ 0 & 0 & 0 \end{pmatrix}, \quad \lambda^3 = \begin{pmatrix} 1 & 0 & 0 \\ 0 & -1 & 0 \\ 0 & 0 & 0 \end{pmatrix},$$

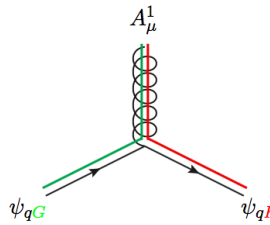
$$\lambda^4 = \begin{pmatrix} 0 & 0 & 1 \\ 0 & 0 & 0 \\ 1 & 0 & 0 \end{pmatrix}, \lambda^5 = \begin{pmatrix} 0 & 0 & -i \\ 0 & 0 & 0 \\ i & 0 & 0 \end{pmatrix}, \lambda^6 = \begin{pmatrix} 0 & 0 & 0 \\ 0 & 0 & 1 \\ 0 & 1 & 0 \end{pmatrix},$$

$$\lambda^7 = \begin{pmatrix} 0 & 0 & 0 \\ 0 & 0 & -i \\ 0 & i & 0 \end{pmatrix}, \lambda^8 = \frac{1}{\sqrt{3}} \begin{pmatrix} 1 & 0 & 0 \\ 0 & 1 & 0 \\ 0 & 0 & -2 \end{pmatrix}.$$

Colour in QCD

Quarks are in the fundamental representation of $SU(3)$. Therefore the Feynman rules for the quark-gluon vertex involve t_{ij}^a where $i, j = 1 \dots N_c$ run over the colours of the quarks (the *degree* of the group), while $a = 1 \dots N_c^2 - 1$ runs over the dimension of the group. Gluons are in the adjoint representation of $SU(3)$, which we denote by the matrices $(F^a)_{bc} = -i f^{abc}$.

The gluons can be regarded as a combination of two coloured lines, as depicted in Fig. 18, or, more precisely, as a combination of colour and anti-colour. Contracting colour indices is graphically equivalent to connecting the



$$\begin{aligned} &\propto -\frac{i}{2}g_s \quad \bar{\psi}_{qR} \quad \lambda^1 \quad \psi_{qG} \\ &= -\frac{i}{2}g_s \quad (\mathbf{1} \ 0 \ 0) \quad \begin{pmatrix} 0 & 1 & 0 \\ 1 & 0 & 0 \\ 0 & 0 & 0 \end{pmatrix} \quad \begin{pmatrix} 0 \\ 1 \\ 0 \end{pmatrix} \end{aligned}$$

Figure 18: Representation of the gluon as a double colour line. *Picture from Ref. [10].*

respective colour (or anticolour) lines. The representation of the quark-gluon vertex in Fig. 18 embodies colour conservation, whereby the colour-anticolour quantum numbers carried by the $q\bar{q}$ pair are transferred to the gluon. The eight gluons can be regarded as all possible colour-anticolour combinations, where the combination corresponding to λ^8 would be $\frac{1}{\sqrt{6}}(r\bar{r} + g\bar{g} - 2b\bar{b})$ (with r : red, g : green, b : blue). Note that the singlet combination $\frac{1}{\sqrt{3}}(r\bar{r} + g\bar{g} + b\bar{b})$ does not occur for the gluon because it cannot mediate colour.

From a group theory point of view, we have an octet and a singlet when forming the product of the fundamental representations $[3]$ and $[\bar{3}]$ for quarks and antiquarks, respectively: $[3] \otimes [\bar{3}] = [8] \oplus [1]$, and the gluons belong to the $[8]$.

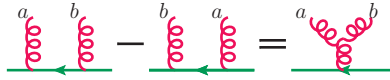
The sums $\sum_{a,j} t_{ij}^a t_{jk}^a$ and $\sum_{a,d} F_{bd}^a F_{dc}^a$ have two free indices in the fundamental and adjoint representation, respectively. One can show that these sums are invariant under $SU(N)$ transformations, and therefore must be proportional to the unit matrix:

$$\sum_{j,a} t_{ij}^a t_{jk}^a = C_F \delta_{ik}, \quad \sum_{a,d} F_{bd}^a F_{dc}^a = C_A \delta_{bc}. \quad (39)$$

The constants C_F and C_A are the eigenvalues of the quadratic *Casimir operator* in the fundamental and adjoint representation, respectively. The Casimirs can be expressed in terms of the number of colours N_c as

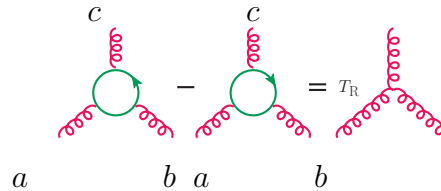
$$C_F = T_R \frac{N_c^2 - 1}{N_c}, \quad C_A = 2 T_R N_c. \quad (40)$$

The commutation relation (33) in the fundamental representation can be represented graphically by



$$t^a t^b - t^b t^a = i f^{abc} t^c$$

Multiplying this commutator first with another colour charge operator, summing over the fermion index and then taking the trace over the fermion line (i.e. multiplying with δ_{ik}) we obtain the representation of the three-gluon vertex as traces of products of colour charges:



$$\text{Trace}(t^a t^b t^c) - \text{Trace}(t^c t^b t^a) = i T_R f^{abc} \quad (41)$$

In the exercises we will see some examples of how to compute the colour algebra structure of a QCD diagram, independent of the kinematics. For example, taking the trace of the identity (δ_{ij} resp. δ_{ab}) in the fundamental resp. in the adjoint representation we obtain

$$\text{Tr}(\delta_{ij}) = N_c, \quad \text{Tr}(\delta_{ab}) = N_c^2 - 1,$$

respectively. Then, using the expressions for the fermion and gluon propagator insertions, we find

$$\text{Tr}(t^a_{ij}) = C_F N_c, \quad \text{Tr}(f^a_{abc}) = C_A (N_c^2 - 1).$$

There is also a very useful identity for the product of two colour matrices in the fundamental representation, occurring when a gluon is exchanged between two quark lines, and following from representing the gluon as a double quark line,

$$t^a_{ij} t^a_{kl} = T_R \left(\begin{array}{c} j \longrightarrow i \\ \text{gluon} \\ k \longleftarrow l \end{array} \right) = T_R \left(\begin{array}{c} j \longrightarrow i \\ \text{double quark} \\ k \longleftarrow l \end{array} - \frac{1}{N_c} \begin{array}{c} j \longrightarrow i \\ \text{crossed quark} \\ k \longleftarrow l \end{array} \right)$$

corresponding to

$$t^a_{ij} t^a_{kl} = T_R \left(\delta_{il} \delta_{kj} - \frac{1}{N_c} \delta_{ij} \delta_{kl} \right). \quad (42)$$

The second term $\sim 1/N_c$ implements the condition that the generators are traceless, and the picture indicates that a gluon which mediates between quarks of the same colour does not exist, because it would be a colour singlet.

Colour decomposition

From eq. (41) it is clear that any tree level diagram for n -gluon scattering can be expressed in terms of traces over generators t^a_{ij} only, as depicted in Fig. 19. This observation leads to the so-called *colour decomposition* of amplitudes, which allows to separate the colour information from the kinematic part of an amplitude. An amplitude for n -gluon scattering can be written as

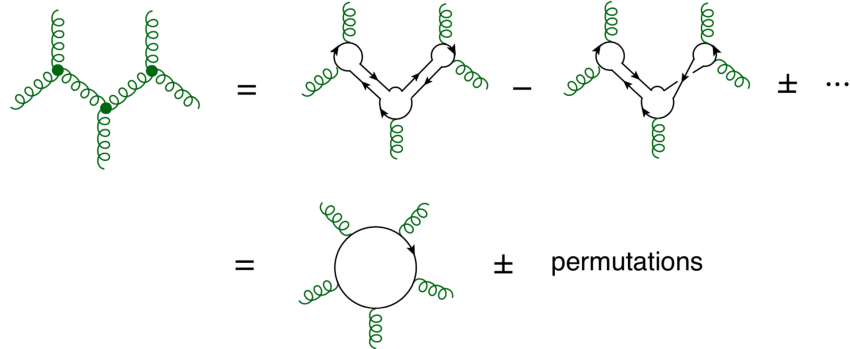


Figure 19: Colour decomposition of tree-level gluon amplitudes. *Figure from Ref. [11].*

$$\mathcal{A}_n^{\text{tree}}(\{k_i, \lambda_i, a_i\}) = g_s^{n-2} \sum_{\sigma \in S_n/Z_n} \text{Tr}(t^{a_{\sigma(1)}} \dots t^{a_{\sigma(n)}}) A_n^{\text{tree}}(\sigma(1^{\lambda_1}), \dots, \sigma(n^{\lambda_n})), \quad (43)$$

where k_i, λ_i are the gluon momenta and helicities, a_i the colour indices and $A_n^{\text{tree}}(1^{\lambda_1}, \dots, n^{\lambda_n})$ are the *partial amplitudes*, which contain all the kinematic information. S_n is the set of all permutations of n objects, while Z_n is the subset of cyclic permutations, which preserves the trace; the latter are excluded in the sum over the set S_n/Z_n .

The advantage of this representation is that the partial amplitudes A_n^{tree} are simpler to calculate than the full amplitude because they are *colour-ordered*: they only receive contributions from diagrams with a particular cyclic ordering of the gluons. This implies that the infrared singularities (related to external massless particles becoming collinear, see later) of the partial amplitudes can only occur in a subset of momentum channels, those with cyclically adjacent momenta. For example, the five-point partial amplitudes $A_5^{\text{tree}}(1^{\lambda_1}, 2^{\lambda_2}, 3^{\lambda_3}, 4^{\lambda_4}, 5^{\lambda_5})$ can only have poles in $s_{12}, s_{23}, s_{34}, s_{45},$ and s_{51} , and not in $s_{13}, s_{24}, s_{35}, s_{41},$ or s_{52} , where $s_{ij} \equiv (k_i + k_j)^2$.

The colour decomposition is not limited to gluons only, it also can be applied when quarks are involved. For example, a tree amplitude with a $q\bar{q}$ pair and otherwise gluons can be written as

$$\mathcal{A}_n^{\text{tree}} = g_s^{n-2} \sum_{\sigma \in S_{n-2}} (t^{a_{\sigma(3)}} \dots t^{a_{\sigma(n)}})_{j_1 i_2} A_n^{\text{tree}}(1_{\bar{q}}^{\lambda_1}, 2_q^{\lambda_2}, \sigma(3^{\lambda_3}), \dots, \sigma(n^{\lambda_n})), \quad (44)$$

where numbers without subscripts refer to gluons.

Using eq.(42), there is yet another possibility to perform the colour decomposition, based on Kronecker δ_{ij} 's only, also called *colour flow decomposition* [12], because it relies on representing all gluons as a double colour line. The computational gain when using colour decomposition to calculate amplitudes with n gluons is illustrated in Fig. 20. At loop level, colour decom-

n	# diagrams	
	partial amplitude	full amplitude
4	3	4
5	10	25
6	36	220
7	133	2485
8	501	34300
9	1991	559405
10	7335	10525900
11	28199	224449225
12	108281	5348843500

Figure 20: Number of diagrams for tree-level n -gluon amplitudes. *Table from Ref. [12].*

position can also be performed [11, 13].

Another advantage of colour decomposition is the possibility to approximate complex calculations by the leading colour approximation, which is a very good approximation for example in the case of di-jet production at NNLO (see Fig. 23).

2.3.2 Experimental evidence for the existence of colour

The colour factors C_F and C_A can indirectly be measured at colliders, for example from jet production cross sections. Jets can be pictured as clusters

of particles (usually hadrons) which are close to each other in phase space, resp. in the detector.

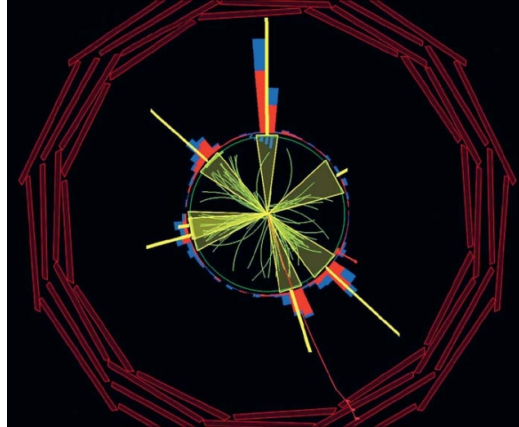


Figure 21: Example of a 6-Jet event measured by CMS. *Source: CERN Courier.*

Fig. 21 shows a 6-jet event measured by CMS, Fig. 22 illustrates how jets at different levels are described, from the partonic interaction to the hadrons seen in the detector.

As the theory predictions for the jet cross sections depend on N_c , these measurements confirm that the number of colours is three.

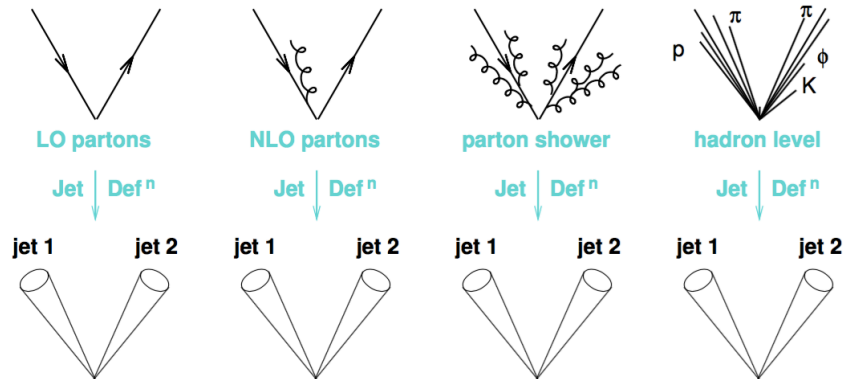


Figure 22: Projections to a 2-jet event at various stages of the theoretical description. *Figure by Gavin Salam.*

As an example, the leading colour contribution to the squared n -gluon matrix elements summed over colours (and helicities) is given by

$$|\mathcal{M}_n|^2 = (g^2 N_c)^{n-2} (N_c^2 - 1) \sum_{\sigma \in S_n/Z_n} \left\{ |\mathcal{A}_n(\sigma(1), \dots, \sigma(n))|^2 + \mathcal{O}\left(\frac{1}{N_c^2}\right) \right\},$$

so if N_c was different, the jet cross sections would change drastically. How well they agree with recent measurements is shown in Fig. 23.

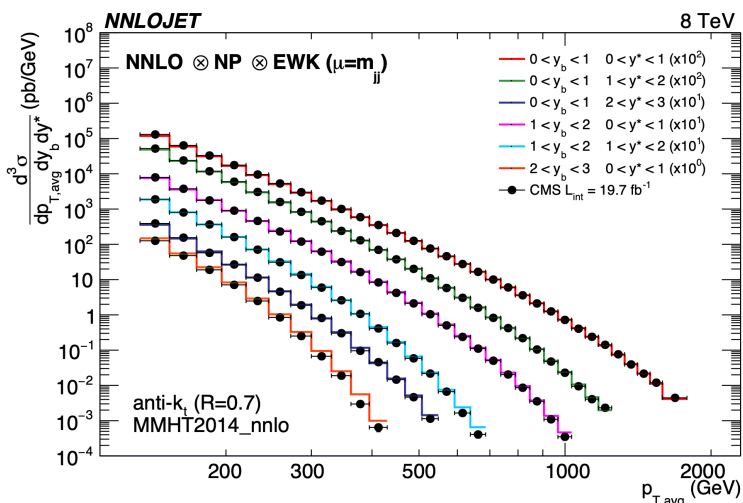


Figure 23: Triple differential two-jet cross sections at NNLO compared to CMS data. Figure from Ref. [14].

A good theoretical description of jets at the LHC is very important. For example, jet+X, two-jet or Z +jet data are important to constrain the PDFs [15] and jet cross sections are used for precision determinations of the strong coupling α_s . Furthermore, as jets are originating from massless partons, there is energy available to go up to very high values in the jet p_T spectrum, ($\mathcal{O}(1TeV)$), which is a kinematic region sensitive to new physics. Jets in combination with missing transverse energy (“missing” in the total transverse energy budget) could be a signal for an unknown heavy particle (for example related to dark matter) decaying into something not visible in the detector.

Hadronic R-ratio

Among the historically early evidences for the existence of 3 colour quantum numbers is the so-called *hadronic R-Ratio*, the total cross section for the production of hadrons in electron-positron collisions, divided by the cross section for the production of a Muon-antimuon pair, as a function of the centre-of-mass energy s :

$$R(s) = \frac{\sigma(e^+e^- \rightarrow \text{hadrons})}{\sigma(e^+e^- \rightarrow \mu^+\mu^-)} . \quad (45)$$

Hadrons are bound states of quarks and gluons, so for the numerator, at microscopic level, this means that a fermion-antifermion pair $f\bar{f}$ is created as soon as the centre-of-mass energy s is sufficient to produce two quarks of mass m_f .

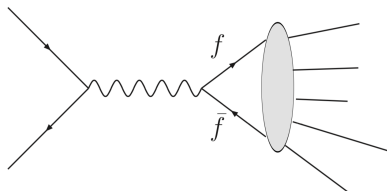


Figure 24: The production of hadrons in e^+e^- collisions via virtual photon exchange.

The interaction proceeds via the exchange of a virtual photon, see Fig. 24 (neglecting Z -boson exchange). The electromagnetic interaction (the photon) only sees the electromagnetic charge e_f of the fermions, be it quarks or leptons. Therefore one would expect that at large energies

$$R(s) = \frac{\sum_{f=u,d,s,c,\dots} \sigma(e^+e^- \rightarrow f\bar{f})}{\sigma(e^+e^- \rightarrow \mu^+\mu^-)} \xrightarrow{s \text{ large}} \sum_{f=u,d,s,c,\dots} e_f^2 \theta(s - 4m_f^2) . \quad (46)$$

However this is not what has been found experimentally! The experimental results agree with the expression

$$R(s) \longrightarrow N_c \sum_{f=u,d,s,c,\dots} e_f^2 \theta(s - 4m_f^2) , \quad (47)$$

with $N_c = 3$.

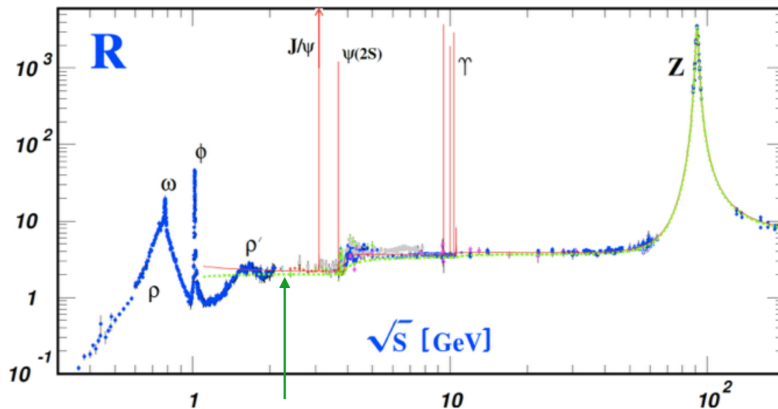


Figure 25: R-Ratio vs. center-of-mass energy. *Figure from Ref. [16].*

Above the bottom quark pair production threshold, we have ($m_b \simeq 4.2$ GeV)

$$R(s) = N_c \sum_{f=u,d,s,c,b} e_f^2 \theta(s - 4m_f^2) = 3 \left(\frac{4}{9} + \frac{1}{9} + \frac{1}{9} + \frac{4}{9} + \frac{1}{9} \right) = \frac{11}{3}. \quad (48)$$

The stepwise increase of the R-ratio can be seen in Fig. 25, even though it is blurred by the resonances ρ, ω, ϕ , etc. In Fig. 26 the quark pair production thresholds without the resonances are shown. The top quark does not show up here, it is heavier than the Z -boson, $m_t \simeq 173$ GeV, and it decays before it hadronizes.

Another example which is often given as an argument for $N_c = 3$ is the decay rate of a neutral pion into two photons:

$$\Gamma(\pi^0 \rightarrow \gamma\gamma) \simeq \alpha^2 \frac{m_\pi^3}{f_\pi^2} (e_u^2 - e_d^2)^2 N_c^2. \quad (49)$$

Note however that there could be cancellations between N_c and a different denominator in the fractional charges of the quarks, for $e_u = (1/N_c + 1)/2$, $e_d = (1/N_c - 1)/2$ the decay rate would be independent of N_c (and a relation between N_c and the fractional charges of the quarks also makes sense in view of anomaly cancellation). Therefore, Eq. (49) alone cannot be seen as a full proof of N_c being equal to 3.

A more theoretical argument for the existence of a colour quantum number is given by the fact that bound states consisting of three quarks, e.g. Δ^{++}

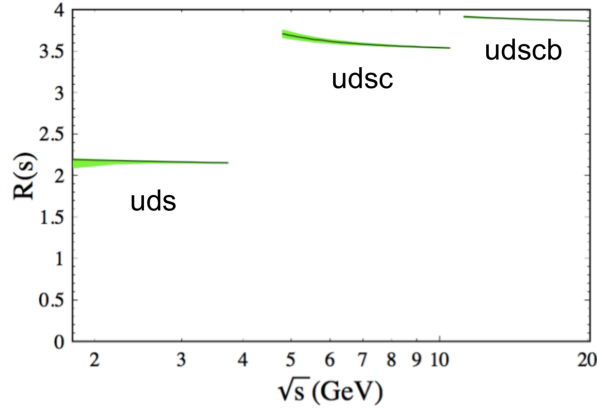


Figure 26: R-ratio without resonance effects. *Figure from Ref. [17].*

consisting of 3 u -quarks, would violate Pauli's exclusion principle if there was no additional quantum number (which implies that this state must be totally antisymmetric in the colour indices).

2.3.3 QCD Lagrangian

An important concept in QCD (and in quantum field theories in general) is the formulation as a *local* gauge theory. This means that the gauge transformation parameter depends itself on x , the position in space-time.

Fermionic part of the QCD Lagrangian

Consider the quark fields $q_f^j(x)$ for just one quark flavour f . The index j labels the colour, $j = 1, \dots, N_c$. Treating the quarks as free Dirac fields, we have

$$\mathcal{L}_q^{(0)}(q_f, m_f) = \sum_{j,k=1}^{N_c} \bar{q}_f^j(x) (i \gamma_\mu \partial^\mu - m_f) \delta_{jk} q_f^k(x), \quad (50)$$

where the Dirac-matrices γ_μ satisfy the anti-commutation relation (Clifford algebra)

$$\{\gamma^\mu, \gamma^\nu\} = 2 g^{\mu\nu}. \quad (51)$$

Now let us apply a group transformation on the fermion fields. It has the form

$$q_k \rightarrow q'_k = U_{kl} q^l, \quad \bar{q}_k \rightarrow \bar{q}'_k = \bar{q}^l U_{lk}^{-1}, \quad (52)$$

with

$$U_{kl} = \exp \left\{ i \sum_{a=1}^{N_c^2-1} t^a \theta^a \right\}_{kl} \equiv \exp \{ i \mathbf{t} \cdot \boldsymbol{\theta} \}_{kl}, \quad (53)$$

where θ^a are the group transformation parameters and $(t^a)_{kl}$ the generators of $SU(N_c)$ in the fundamental representation. The Lagrangian of free Dirac fields remains invariant under this transformation as long as it is a *global* transformation, i.e. as long as the θ^a do not depend on x : $\mathcal{L}_q^{(0)}(q) = \mathcal{L}_q^{(0)}(q')$. However, we aim at *local* gauge transformations, where the gauge transformation parameter θ in Eq. (53) depends on x . In QED, where the underlying gauge group is $U(1)$, a global transformation would just be a phase change. The requirement of a free electron field to be invariant under *local* transformations $\theta = \theta(x)$ leads to the introduction of a *gauge field* A_μ , the photon. The analogous is true for QCD: requiring local gauge invariance under $SU(N_c)$ leads to the introduction of gluon fields A_μ^a .

As the local gauge transformation

$$U(x) = \exp \{ i \mathbf{t} \cdot \boldsymbol{\theta}(x) \} \quad (54)$$

depends on x , the derivative of the transformed quark field $q'(x)$ reads

$$\partial_\mu q'(x) = \partial_\mu (U(x)q(x)) = U(x)\partial_\mu q(x) + (\partial_\mu U(x)) q(x). \quad (55)$$

To keep \mathcal{L}_q gauge invariant, we can remedy the situation caused by the second term above by introducing the coupling to a gauge field which transforms accordingly. We define a *covariant derivative* D^μ , depending on A_a^μ , by

$$(D^\mu[A])_{ij} = \delta_{ij}\partial^\mu + i g_s t_{ij}^a A_a^\mu, \quad (56)$$

or, without index notation

$$\mathbf{D}^\mu[\mathbf{A}] = \partial^\mu + i g_s \mathbf{A}^\mu, \quad (57)$$

where $\mathbf{A}^\mu = t^a A_a^\mu$ (sum over $a = 1 \dots N_c^2 - 1$ understood). The fields A_a^μ are the *gluons*. The Lagrangian corresponding to this “minimal coupling” of

a gluon field reads

$$\mathcal{L}_q(q_f, m_f) = \sum_{j,k=1}^{N_c} \bar{q}_f^j(x) (i \gamma_\mu \mathbf{D}^\mu[\mathbf{A}] - m_f)_{jk} q_f^k(x). \quad (58)$$

To keep this Lagrangian invariant under local gauge transformations, we therefore must have

$$\mathbf{D}^\mu[\mathbf{A}']q'(x) \stackrel{!}{\rightarrow} U \left(\mathbf{D}^\mu[\mathbf{A}]q(x) \right), \quad (59)$$

where the transformation of the expression $\mathbf{D}^\mu[\mathbf{A}]q(x)$ is given by

$$(\partial_\mu + ig_s \mathbf{A}_\mu(x))q(x) \rightarrow (\partial_\mu + ig_s \mathbf{A}'_\mu(x))Uq(x). \quad (60)$$

Eq.(60) gives a condition on $\mathbf{A}'_\mu(x)$, which can be derived as an exercise. The result is that the gluon fields need to transform under general $SU(N_c)$ transformations as follows:

$$\mathbf{A}'_\mu = U(x)\mathbf{A}_\mu U^{-1}(x) + \frac{i}{g_s}(\partial_\mu U(x))U^{-1}(x). \quad (61)$$

Purely gluonic part of the QCD Lagrangian

The purely gluonic part of the QCD Lagrangian can be described by the so-called Yang-Mills Lagrangian (C. N. Yang, R. Mills, 1954)

$$\mathcal{L}_{\text{YM}} = -\frac{1}{4}F_{\mu\nu}^a F^{a,\mu\nu}, \quad (62)$$

where the non-Abelian field strength tensor $F_{\mu\nu}^a$ is given by

$$F_{\mu\nu}^a = \partial_\mu A_\nu^a - \partial_\nu A_\mu^a - g_s f^{abc} A_\mu^b A_\nu^c. \quad (63)$$

We can also express everything in terms of $\mathbf{A}^\mu = t^a A_\mu^a$ and write the field strength tensor as

$$\mathbf{F}_{\mu\nu}(x) = \sum_{a=1}^{N_c^2-1} F_{\mu\nu}^a(x) t^a = \frac{i}{g_s} [\mathbf{D}_\mu, \mathbf{D}_\nu], \quad (64)$$

which implies

$$\mathcal{L}_{\text{YM}} = -\frac{1}{4}F_{\mu\nu}^a F^{a,\mu\nu} = -\frac{1}{2}\text{Trace}[\mathbf{F}_{\mu\nu}\mathbf{F}^{\mu\nu}]. \quad (65)$$

Note that the term proportional to f^{abc} in the expression for $F_{\mu\nu}^a$, which reflects the non-Abelian structure and is not present in QED, leads to terms with 3 or 4 gluon fields in the Lagrangian and therefore to self-interactions between the gluons.

So finally we obtain for the “classical” QCD Lagrangian

$$\begin{aligned} \mathcal{L}_c &= \mathcal{L}_{\text{YM}} + \mathcal{L}_q \\ &= -\frac{1}{4} F_{\mu\nu}^a F^{a,\mu\nu} + \sum_{j,k=1}^{N_c} \bar{q}_f^j(x) (i \gamma_\mu \mathbf{D}^\mu[\mathbf{A}] - m_f)_{jk} q_f^k(x). \end{aligned} \quad (66)$$

Gauge fixing

We are not quite there yet with the complete QCD Lagrangian. The “classical” QCD Lagrangian \mathcal{L}_c contains degenerate field configurations (i.e. they are equivalent up to gauge transformations). This leads to the fact that the bilinear operator in the gluon fields is not invertible, such that it is not possible to construct a propagator for the gluon fields. The propagator is usually derived from the bilinear term in the fields in the path integral for free fields, with the generating functional

$$Z_0[J] = \int \mathcal{D}A_\mu(x) e^{i \int d^4x [\frac{1}{2} A_\mu^a(x) (g^{\mu\nu} \square - \partial^\mu \partial^\nu) A_\nu^b(x) \delta_{ab} + J_\mu^a A_\mu^a]}. \quad (67)$$

In momentum space this leads to the following condition for the propagator $\Delta_{\mu\nu}(p)$, where we suppress colour indices as the propagator is diagonal in colour space, i.e. we leave out overall factors δ^{ab} :

$$i \Delta_{\mu\rho}(p) [p^2 g^{\rho\nu} - p^\rho p^\nu] = g_\mu^\nu. \quad (68)$$

However, we also have

$$[p^2 g^{\rho\nu} - p^\rho p^\nu] p_\nu = 0, \quad (69)$$

which means that the matrix $[p^2 g^{\rho\nu} - p^\rho p^\nu]$ is not invertible because it has at least one eigenvalue equal to zero. We have to remove the physically equivalent configurations from the classical Lagrangian. This is called *gauge fixing*. We can achieve this by imposing a constraint on the fields A_μ^a , adding a term to the Lagrangian with a Lagrange multiplier.

For example, *covariant gauges* are defined by the requirement $\partial_\mu A^\mu(x) = 0$ for any x . Adding

$$\mathcal{L}_{\text{GF}} = -\frac{1}{2\lambda} (\partial_\mu A^\mu)^2, \quad \lambda \in \mathbb{R},$$

to \mathcal{L} , the action S remains the same. The bilinear term then has the form

$$i \left(p^2 g^{\mu\nu} - \left(1 - \frac{1}{\lambda}\right) p^\mu p^\nu \right),$$

with inverse

$$\Delta_{\mu\nu}(p) = \frac{-i}{p^2 + i\varepsilon} \left[g_{\mu\nu} - (1 - \lambda) \frac{p_\mu p_\nu}{p^2} \right]. \quad (70)$$

The so-called $i\varepsilon$ prescription ($\varepsilon > 0$) shifts the poles of the propagator slightly off the real p^0 -axis (where p^0 is the energy component) and will become important later when we consider loop integrals. It ensures the correct causal behaviour of the propagators.

Of course, physical results must be independent of λ . Choosing $\lambda = 1$ is called *Feynman gauge*, $\lambda = 0$ is called *Landau gauge*.

In covariant gauges unphysical degrees of freedom (longitudinal and time-like polarisations) also propagate. The effect of these unwanted degrees of freedom is cancelled by the ghost fields, which are coloured complex scalars obeying Fermi statistics. Unphysical degrees of freedom and the ghost fields can be avoided by choosing *axial gauges* (also called *physical gauges*). The axial gauge is defined by introducing an arbitrary vector n^μ with $p \cdot n \neq 0$, to impose the constraint

$$\mathcal{L}_{\text{GF}} = -\frac{1}{2\alpha} (n^\mu A_\mu)^2,$$

which leads to

$$\Delta_{\mu\nu}(p, n) = \frac{-i}{p^2 + i\varepsilon} \left(g_{\mu\nu} - \frac{p_\mu n_\nu + n_\mu p_\nu}{p \cdot n} + \frac{n^2 p_\mu p_\nu}{(p \cdot n)^2} \right).$$

A convenient choice is $n^2 = 0$, called *light-cone gauge*. Note that we have

$$\Delta_{\mu\nu}(p, n) p^\mu = 0, \quad \Delta_{\mu\nu}(p, n) n^\mu = 0.$$

Thus, only 2 degrees of freedom propagate (transverse ones in the $n^\mu + p^\mu$ rest frame). The price to pay by choosing an axial gauge instead of a covariant

one is that the propagator looks more complicated and that it diverges when p^μ becomes parallel to n^μ . In the light-cone gauge we have

$$\begin{aligned}\Delta_{\mu\nu}(p, n) &= \frac{i}{p^2 + i\varepsilon} d_{\mu\nu}(p, n) \\ d_{\mu\nu}(p, n) &= -g_{\mu\nu} + \frac{p_\mu n_\nu + n_\mu p_\nu}{p \cdot n} = \sum_{\lambda=1,2} \epsilon_\mu^\lambda(p) (\epsilon_\nu^\lambda(p))^* ,\end{aligned}\quad (71)$$

where $\epsilon_\mu^\lambda(p)$ is the polarisation vector of the gluon field with momentum p and polarisation λ . This means that only the two physical polarisations ($\lambda = 1, 2$) propagate. In Feynman gauge, we have

$$\sum_{\lambda=0}^3 \epsilon_\mu^\lambda(p) (\epsilon_\nu^\lambda(p))^* = -g_{\mu\nu} ,\quad (72)$$

where the polarisation sum also runs over non-transverse gluon polarisations, which can occur in loops and will be cancelled by the corresponding loops involving ghost fields.

Faddeev-Popov ghost fields

The introduction of a gauge fixing constraint is achieved by inserting

$$1 = \int \mathcal{D}\theta(x) \delta(G^a(A^\theta) - h^a(x)) \det\left(\frac{\delta G^a(A^\theta)}{\delta\theta}\right)\quad (73)$$

(where A^θ denotes all fields which are equivalent through a gauge transformation involving the group parameter θ), into the generating functional $Z[J]$, for example $h^a(x) = \partial^\mu A_\mu^a(x)$ in covariant gauges. The determinant $\det\left(\frac{\delta G^a(A^\theta)}{\delta\theta}\right) =: \Delta_{FP}(A)$ can be written as functional integral over anti-commuting fields $\eta^a(x), \bar{\eta}^b(x)$.

$$\begin{aligned}\Delta_{FP}(A) &= \int \mathcal{D}\bar{\eta}\mathcal{D}\eta e^{i\int d^4x d^4y \bar{\eta}^a(x) M_{ab}(x,y) \eta^b(y)} \\ \text{with } M_{ab}(x,y) &= \frac{\delta G^a(A^\theta(x))}{\delta\theta^b(y)} .\end{aligned}\quad (74)$$

The fields $\bar{\eta}^a(x), \eta^b(x)$ are the so-called *Faddeev-Popov*-fields or *ghost* fields, they are complex scalar fields, which however obey Fermi-statistics, so they anti-commute, and cannot occur as external states.

The additional term in the Lagrangian as a result of the procedure sketched above reads

$$\mathcal{L}_{FP} = \bar{\eta}_a M^{ab} \eta_b . \quad (75)$$

In Feynman gauge, the operator M^{ab} (also called Faddeev-Popov matrix) is given by

$$M_{Feyn}^{ab} = \delta^{ab} \partial_\mu \partial^\mu + g_s f^{abc} A_\mu^c \partial^\mu . \quad (76)$$

Here we can see that in QED (or another Abelian gauge theory) the second term is absent, such that the Faddeev-Popov determinant $\det M$ does not depend on any field and therefore can be absorbed into the normalisation of the path integral, such that no ghost fields are needed in Abelian gauge theories.

In the light-cone gauge, the Faddeev-Popov matrix becomes

$$M_{LC}^{ab} = \delta^{ab} n_\mu \partial^\mu + g_s f^{abc} n_\mu A_c^\mu , \quad (77)$$

such that, due to the gauge fixing condition $n \cdot A = 0$, the matrix is again independent of the gauge field and therefore can be absorbed into the normalisation, such that no ghost fields propagate.

So finally we have derived the full QCD Lagrangian

$$\boxed{\mathcal{L}_{QCD} = \mathcal{L}_{YM} + \mathcal{L}_q + \mathcal{L}_{GF} + \mathcal{L}_{FP} .} \quad (78)$$

2.3.4 QCD Feynman rules

Feynman rules are something like a Lego play box containing pieces that can be assembled to an expression describing a particle process, like the scattering of elementary particles or the decay of a particle. They arise from the interaction terms in the action, resp. the Lagrangian. There are also automated tools that can derive Feynman rules from a given Lagrangian, see e.g. [18].

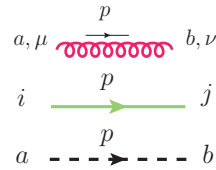
We will not derive the QCD Feynman rules from the action, but just state them below. (The pictures are partly taken from Ref. [19]).

Propagators: ($i\varepsilon$ prescription understood)

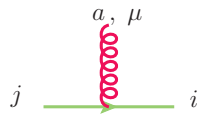
gluon propagator: $\Delta_{\mu\nu}^{ab}(p) = \delta^{ab} \Delta_{\mu\nu}(p)$

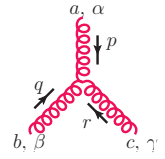
quark propagator: $\Delta_q^{ij}(p) = \delta^{ij} i \frac{\not{p} + m}{p^2 - m^2}$

ghost propagator: $\Delta^{ab}(p) = \delta^{ab} \frac{i}{p^2}$

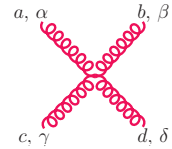


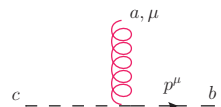
Vertices:

quark-gluon: $\Gamma_{gq\bar{q}}^{\mu,a} = -i g_s (t^a)_{ij} \gamma^\mu$ 

three-gluon: $\Gamma_{\alpha\beta\gamma}^{abc}(p, q, r) = -i g_s (F^a)_{bc} V_{\alpha\beta\gamma}(p, q, r)$ 

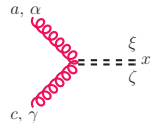
$V_{\alpha\beta\gamma}(p, q, r) = (p - q)_\gamma g_{\alpha\beta} + (q - r)_\alpha g_{\beta\gamma} + (r - p)_\beta g_{\alpha\gamma}, \quad p^\alpha + q^\alpha + r^\alpha = 0$

four-gluon: $\Gamma_{\alpha\beta\gamma\delta}^{abcd} = -i g_s^2 \begin{bmatrix} +f^{xac} f^{xbd} (g_{\alpha\beta} g_{\gamma\delta} - g_{\alpha\delta} g_{\beta\gamma}) \\ +f^{xad} f^{xcb} (g_{\alpha\gamma} g_{\beta\delta} - g_{\alpha\beta} g_{\gamma\delta}) \\ +f^{xab} f^{xdc} (g_{\alpha\delta} g_{\beta\gamma} - g_{\alpha\gamma} g_{\beta\delta}) \end{bmatrix}$ 

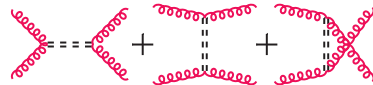
ghost-gluon: $\Gamma_{g\eta\bar{\eta}}^{\mu,a} = -i g_s (F^a)_{bc} p^\mu$ 

The four-gluon vertex differs from the rest of the Feynman rules in the sense that it is not in a factorised form of a colour factor and a kinematic part carrying the Lorentz indices. This is an inconvenient feature because it prevents the separate summation over colour and Lorentz indices and complicates automation. We can however circumvent this problem by introducing an auxiliary field with propagator

$a \overset{\gamma}{=} \overset{\delta}{=} b = -\frac{i}{2} \delta^{ab} (g^{\alpha\beta} g^{\gamma\delta} - g^{\alpha\delta} g^{\beta\gamma}),$
that couples only to the gluon with vertex

 $= i \sqrt{2} g_s f^{xac} g^{\alpha\xi} g^{\gamma\zeta}.$

We can check that a single four-gluon vertex can be written as a sum of three graphs as shown below, for which the summations over colour and Lorentz indices factorize.



Finally, we have to supply the following factors for incoming and outgoing

particles (see Fig. 27)

- outgoing fermion: $\bar{u}(p)$
- incoming fermion: $u(p)$
- outgoing vector boson: $\epsilon_\mu^\lambda(p)^*$
- outgoing antifermion: $v(p)$
- incoming antifermion: $\bar{v}(p)$
- incoming vector boson: $\epsilon_\mu^\lambda(p)$.

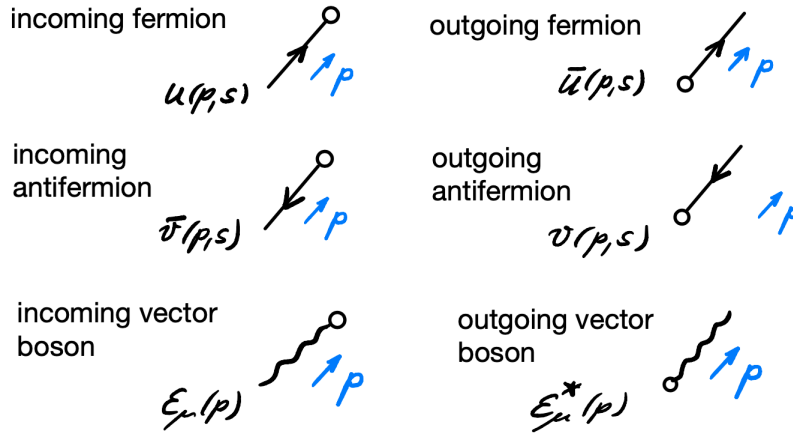


Figure 27: Conventions for spinors with momentum p and spin s and polarisation vectors $\epsilon_\mu(p)$.

3 Example: top quark production

3.1 Phenomenology

The top quark is special because it is so much heavier than the other quarks ($m_t \simeq 173 \text{ GeV}$, $m_b \simeq 4.2 \text{ GeV}$). Therefore the top quark decays before it hadronizes, almost entirely by $t \rightarrow Wb$.

The phenomenological importance of top quarks has many aspects:

- The top quark mass enters many observables and is important to study the vacuum stability of the universe, see Figs. 29, 30.
- It has a large coupling to the Higgs boson, therefore $t\bar{t}H$ and tH production are important processes to constrain the Higgs-top Yukawa coupling and to measure the CP properties of the coupling.

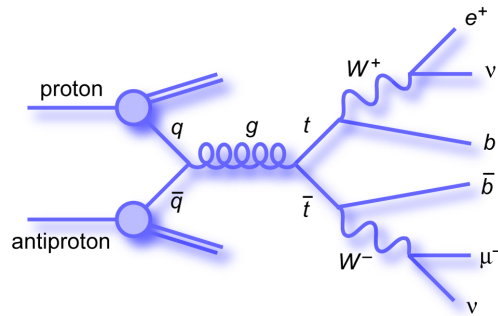


Figure 28: Example Feynman diagram for top quark pair production and decay at the Tevatron ($p\bar{p}$ collisions), where the top quark has been discovered 1995. Source: <https://www-d0.fnal.gov/Run2Physics/top/>

- Inclusion of top quark pair production data in PDF fits reduce the uncertainties on the gluon PDF significantly.
- Physics beyond the SM is likely to manifest itself in the third generation.

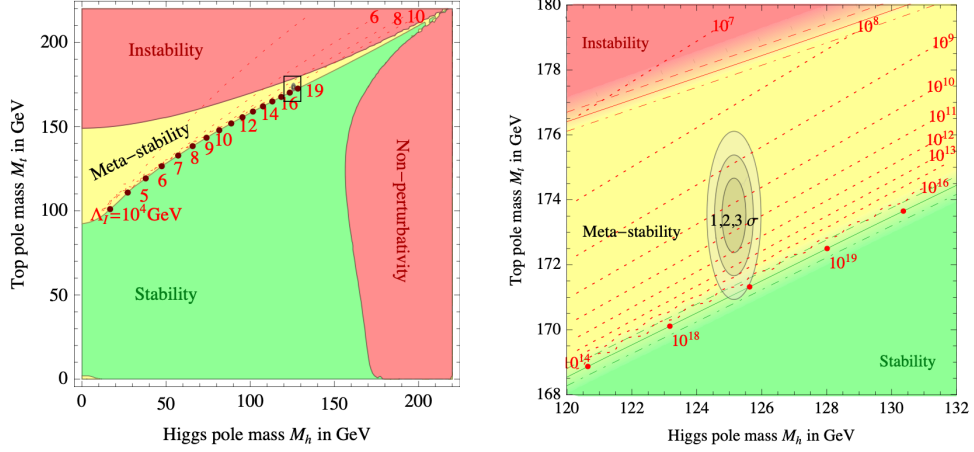


Figure 29: Dependence of vacuum stability on the top quark and Higgs masses. Figures from Ref. [20].

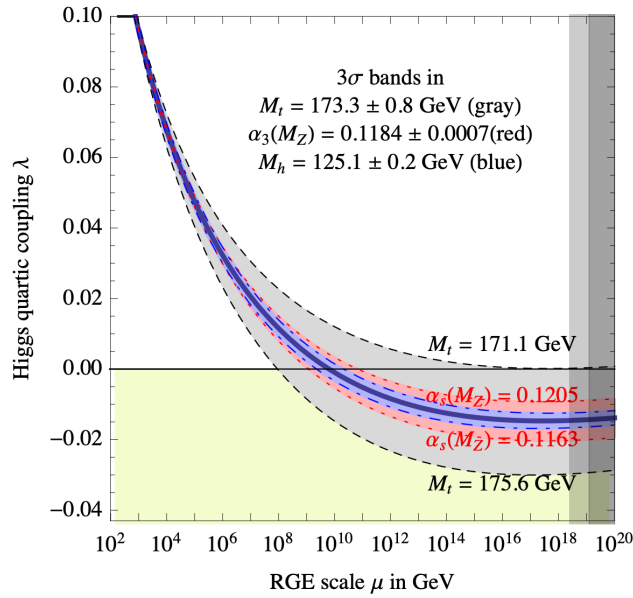


Figure 30: Running of the Higgs quartic self-coupling. Figure from Ref. [20].

3.2 Top quark pair production

The LO Feynman diagrams contribution to top quark pair production are shown in Fig. 31.

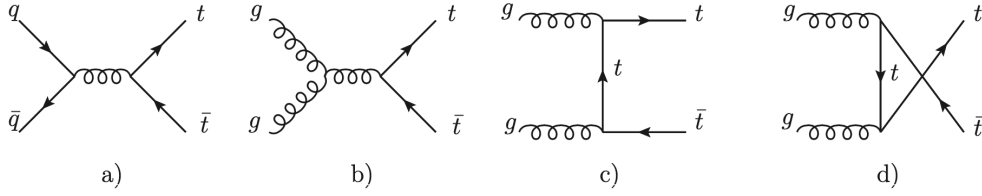


Figure 31: LO Feynman diagrams for top quark pair production.

Top quark pair production is measured at the LHC in several channels: each W -boson can decay both leptonically or hadronically, therefore the signature for top quark pair production consists of two b -jets plus either of the following

- (a) two leptons, $\sim 9\%$
- (b) lepton+jets, $\sim 46\%$
- (c) all hadronic, $\sim 45\%$.

The leptonic decay is also characterised by missing E_T , as the neutrinos escape undetected.

The top quark width is given at LO by

$$\Gamma_t = \frac{G_F m_t^3}{8\pi\sqrt{2}} \left[(1 - \beta^2)^2 + \omega^2(1 + \beta^2) - 2\omega^4 \right] \sqrt{\lambda(1, \beta^2, \omega^2)} \simeq 1.5 \text{ GeV} ,$$

$$\beta = m_b/m_t , \quad \omega = m_W/m_t . \quad (79)$$

It is important to note that most theoretical descriptions of top quark pair production use the so-called *narrow width approximation (NWA)*, which separates the calculation into $t\bar{t}$ production and subsequent decay of each top quark. However, considering for example the dilepton channel, $pp \rightarrow W^+W^-b\bar{b} \rightarrow (e^+\nu_e)(\mu^-\bar{\nu}_\mu)b\bar{b}$, the final state of two leptons and two b -jets can also originate from processes that do not proceed via the production of a top quark pair, see Fig. 32. Processes involving two resonant top quarks

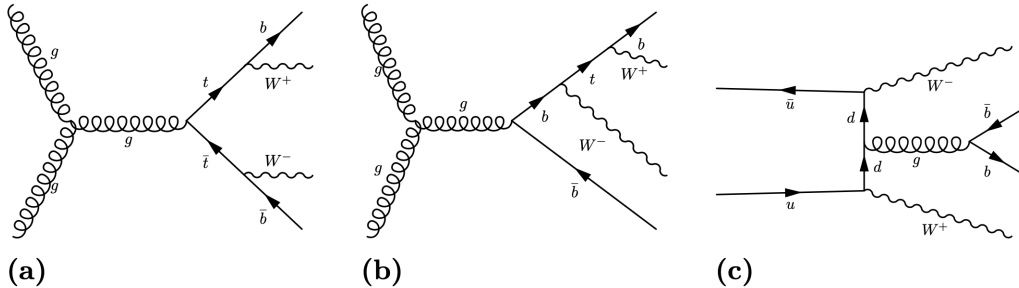


Figure 32: Representative LO Feynman diagrams for (a) resonant, (b) singly resonant and (c) non-resonant contributions. Figure from [21].

are called “doubly resonant”, those involving one top decaying into Wb are called “singly resonant” and there are also non-resonant diagrams. At NLO, there can be also non-factorising contributions, see Fig. 33 (b).

The narrow width approximation (NWA) is motivated by the fact that, in the limit $\Gamma_t \rightarrow 0$, the denominator of the top quark propagator can be written as

$$\lim_{\Gamma_t \rightarrow 0} \frac{1}{(p_t^2 - m_t^2)^2 + m_t^2 \Gamma_t^2} = \frac{\pi}{m_t \Gamma_t} \delta(p_t^2 - m_t^2) + \mathcal{O}\left(\frac{\Gamma_t}{m_t}\right). \quad (80)$$

Since this approximation introduces a factor of $1/\Gamma_t$ for each top quark resonance, singly resonant and non-resonant contributions are suppressed in the $\Gamma_t \rightarrow 0$ limit. Consequently, one only keeps the Feynman diagrams where two top quarks can become resonant, because only those are proportional to $1/\Gamma_t^2$. In the $\Gamma_t \rightarrow 0$ limit, the full process therefore factorizes into top quark pair production and decay, i.e. $pp \rightarrow t\bar{t} \rightarrow W^+b W^-\bar{b}$.

Experimentally, one tries to suppress the unwanted contributions by so-called *kinematic cuts*, for example requiring $p_T^{lb} > 120$ GeV, where p_T^{lb} denotes the mean transverse momentum of the two lepton–b-quark systems, and a separation between the leptons and the jets.

Fig. 34 shows the difference in the distribution of the invariant mass of a lepton and a b-jet, $m_{lb} = (p_l + p_{b,\text{jet}})^2$ for various theoretical descriptions.

3.3 Higgs plus top quarks

The process $t\bar{t}H$ is particularly interesting due to its direct sensitivity to the top-Yukawa coupling y_t . However, this process suffers from large system-

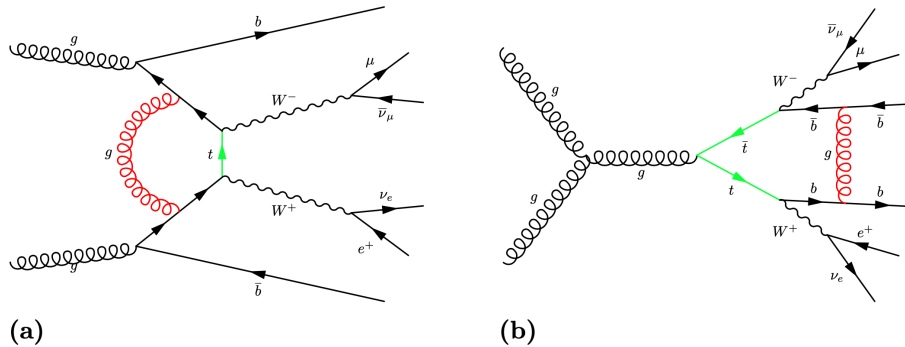


Figure 33: Representative NLO Feynman diagrams for (a) non-resonant, and (b) non-factorising contributions. Figure from Ref. [22].

atic uncertainties due to the very complicated final states. Currently the combination with $H \rightarrow \gamma\gamma$ is the most promising channel [23], however the $H \rightarrow b\bar{b}$ channel is of increasing importance as deep learning methods gain momentum as a way to improve the signal-to-background ratio.

The $H \rightarrow \gamma\gamma$ decay channel of the $t\bar{t}H$ process is particularly well suited to measure a possible CP-violating phase of the top Yukawa coupling and experimental constraints are already available [24, 25].

Using single top plus Higgs production to probe the CP-properties of the top Yukawa coupling is important to determine the sign of the (potentially anomalous) coupling.

3.4 New Physics effects (effective field theory)

Assuming that the SM Lagrangian is only the leading approximation of a more complete theory, consisting of operators up to dimension 4, one can parametrise the effects of interactions taking place at higher energy scales by an effective field theory (EFT) that also includes higher-dimensional operators. It is based on the assumption that a more complete theory involves particles that are much heavier than the electroweak scale ($v \sim 250$ GeV), and therefore the heavy degrees of freedom can be parametrised by operators of mass dimension larger than four, in a systematic expansion in inverse powers of a dimensionful scale Λ , the scale where New Physics effects become dominant.

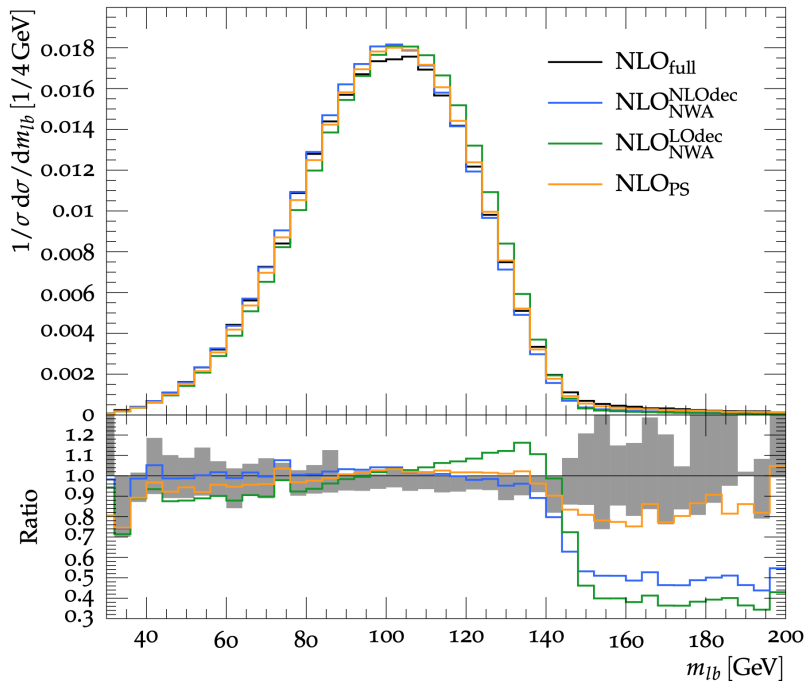


Figure 34: Normalised differential cross sections for the invariant mass m_{lb} at the 13 TeV LHC for four different theoretical descriptions. Figure from Ref. [22].

We may write the Standard Model Effective Field Theory (SMEFT) Lagrangian as

$$\mathcal{L}_{\text{SMEFT}} = \mathcal{L}_{\text{SM}} + \sum_i \frac{C_i^{(6)}}{\Lambda^2} \mathcal{O}_i^{\text{dim6}} + \mathcal{O}\left(\frac{1}{\Lambda^3}\right), \quad (81)$$

where C_i are dimensionless Wilson coefficients, and we have omitted the contribution at dimension 5, which can only be a lepton number-violating operator, $\mathcal{L}_{\text{dim5}} \simeq \bar{L}^i \phi^c (\phi^c L^j)^\dagger$. The Lagrangian $\mathcal{L}_{\text{SMEFT}}$ is not renormalisable in the strict sense (which means, the theory is determined by a fixed number of renormalisation parameters), however the requirement that the EFT is closed under renormalisation order by order in the asymptotic expansion, still can be fulfilled, even though the number of counterterms will grow with the order.

The upper limit of the sum in Eq. (81) is 2499 if no assumptions on flavour-

		1 : X^3	2 : H^6	3 : $H^4 D^2$	5 : $\psi^2 H^3 + \text{h.c.}$				
Gauge Fields	Q_G	$f^{ABC} G_\mu^{A\nu} G_\nu^{B\rho} G_\rho^{C\mu}$	Higgs Fields	Q_H	$(H^\dagger H)^3$	$Q_{H\Box}$	$(H^\dagger H)\Box(H^\dagger H)$	Q_{eH}	$(H^\dagger H)(\bar{l}_p e_r H)$
	$Q_{\tilde{G}}$	$f^{ABC} \tilde{G}_\mu^{A\nu} G_\nu^{B\rho} G_\rho^{C\mu}$		Q_{HD}	$(H^\dagger D^\mu H)^* (H^\dagger D_\mu H)$	Q_{uH}	$(H^\dagger H)(\bar{q}_p u_r \tilde{H})$		
	Q_W	$\epsilon^{IJK} W_\mu^{I\nu} W_\nu^{J\rho} W_\rho^{K\mu}$		Q_{dH}	$(H^\dagger H)(\bar{q}_p d_r H)$				
	$Q_{\tilde{W}}$	$\epsilon^{IJK} \tilde{W}_\mu^{I\nu} W_\nu^{J\rho} W_\rho^{K\mu}$							
Gauge & Higgs Fields	4 : $X^2 H^2$		6 : $\psi^2 XH + \text{h.c.}$		fermion	7 : $\psi^2 H^2 D$			
	Q_{HG}	$H^\dagger H G_{\mu\nu}^A G^{A\mu\nu}$	Q_{eW}	$(\bar{l}_p \sigma^{\mu\nu} e_r) \tau^I H W_{\mu\nu}^I$	$Q_{Hl}^{(1)}$	$(H^\dagger i \overleftrightarrow{D}_\mu H)(\bar{l}_p \gamma^\mu l_r)$			
	$Q_{H\tilde{G}}$	$H^\dagger H \tilde{G}_{\mu\nu}^A G^{A\mu\nu}$	Q_{eB}	$(\bar{l}_p \sigma^{\mu\nu} e_r) H B_{\mu\nu}$	$Q_{Hl}^{(3)}$	$(H^\dagger i \overleftrightarrow{D}_\mu^I H)(\bar{l}_p \tau^I \gamma^\mu l_r)$			
	Q_{HW}	$H^\dagger H W_{\mu\nu}^I W^{I\mu\nu}$	Q_{uG}	$(\bar{q}_p \sigma^{\mu\nu} T^A u_r) \tilde{H} G_{\mu\nu}^A$	Q_{He}	$(H^\dagger i \overleftrightarrow{D}_\mu H)(\bar{e}_p \gamma^\mu e_r)$			
	$Q_{H\tilde{W}}$	$H^\dagger H \tilde{W}_{\mu\nu}^I W^{I\mu\nu}$	Q_{uW}	$(\bar{q}_p \sigma^{\mu\nu} u_r) \tau^I \tilde{H} W_{\mu\nu}^I$	$Q_{Hq}^{(1)}$	$(H^\dagger i \overleftrightarrow{D}_\mu H)(\bar{q}_p \gamma^\mu q_r)$			
	Q_{HB}	$H^\dagger H B_{\mu\nu} B^{\mu\nu}$	Q_{uB}	$(\bar{q}_p \sigma^{\mu\nu} u_r) \tilde{H} B_{\mu\nu}$	$Q_{Hq}^{(3)}$	$(H^\dagger i \overleftrightarrow{D}_\mu^I H)(\bar{q}_p \tau^I \gamma^\mu q_r)$			
	$Q_{H\tilde{B}}$	$H^\dagger H \tilde{B}_{\mu\nu} B^{\mu\nu}$	Q_{dG}	$(\bar{q}_p \sigma^{\mu\nu} T^A d_r) H G_{\mu\nu}^A$	Q_{Hu}	$(H^\dagger i \overleftrightarrow{D}_\mu H)(\bar{u}_p \gamma^\mu u_r)$			
	Q_{HWB}	$H^\dagger \tau^I H W_{\mu\nu}^I B^{\mu\nu}$	Q_{dW}	$(\bar{q}_p \sigma^{\mu\nu} d_r) \tau^I H W_{\mu\nu}^I$	Q_{Hd}	$(H^\dagger i \overleftrightarrow{D}_\mu H)(\bar{d}_p \gamma^\mu d_r)$			
$Q_{H\tilde{W}B}$	$H^\dagger \tau^I H \tilde{W}_{\mu\nu}^I B^{\mu\nu}$	Q_{dB}	$(\bar{q}_p \sigma^{\mu\nu} d_r) H B_{\mu\nu}$	$Q_{Hud} + \text{h.c.}$	$i(\tilde{H}^\dagger D_\mu H)(\bar{u}_p \gamma^\mu d_r)$				

Figure 35: Examples of dimension 6 operators. Figure from Viviana Cavaliere, talk at KITP2021.

symmetries of the New Physics sector are made. If the flavour symmetry of the SM is assumed, the number of operators reduces to about 70. Some dimension-6 operators \mathcal{O}_i in the so-called Warsaw basis are given in Fig. 35 (adapted from Ref. [26]).

Examples of operators mediating interactions not present in the SM in $t\bar{t}H$ production are shown in Fig. 36.

Figs. 37 and 38 show how a combined fit based on several processes can help to constrain the higher dimensional operators. Note that processes like $pp \rightarrow H$, $pp \rightarrow H j$ and $pp \rightarrow HH$, also involve Higgs-top and Higgs-gluon operators.

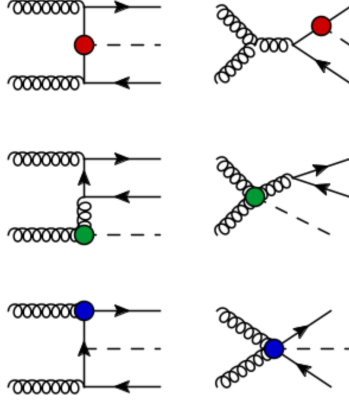


Figure 36: Operators involved in $t\bar{t}H$ production. Figure from Ref. [27].

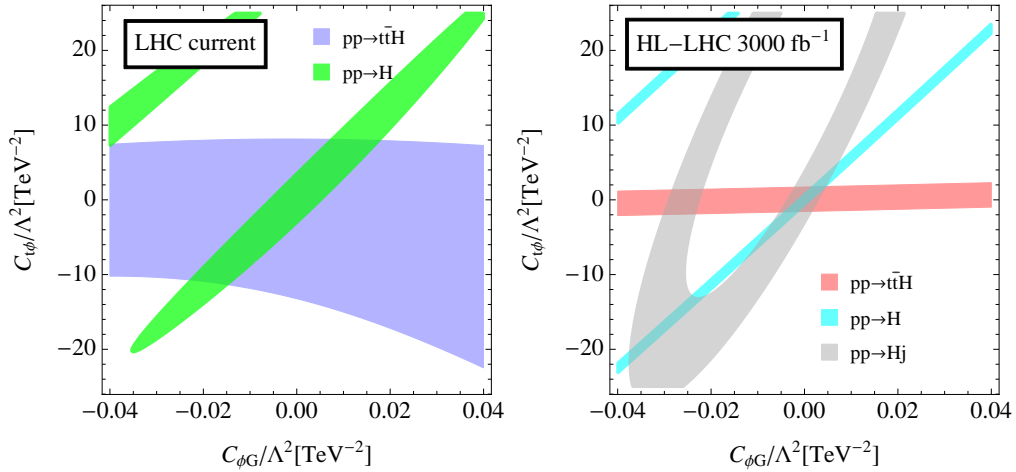


Figure 37: Allowed region in the $C_{t\phi}$ - $C_{\phi G}$ plane at 95% confidence level, where $C_{t\phi}$ and $C_{\phi G}$ denote the Wilson coefficients of the top-Higgs and Higgs-gluon operators, respectively. Left: current constraints. Right: Projection for the HL-LHC. The theoretical uncertainties are not included. Figures from Ref. [27].

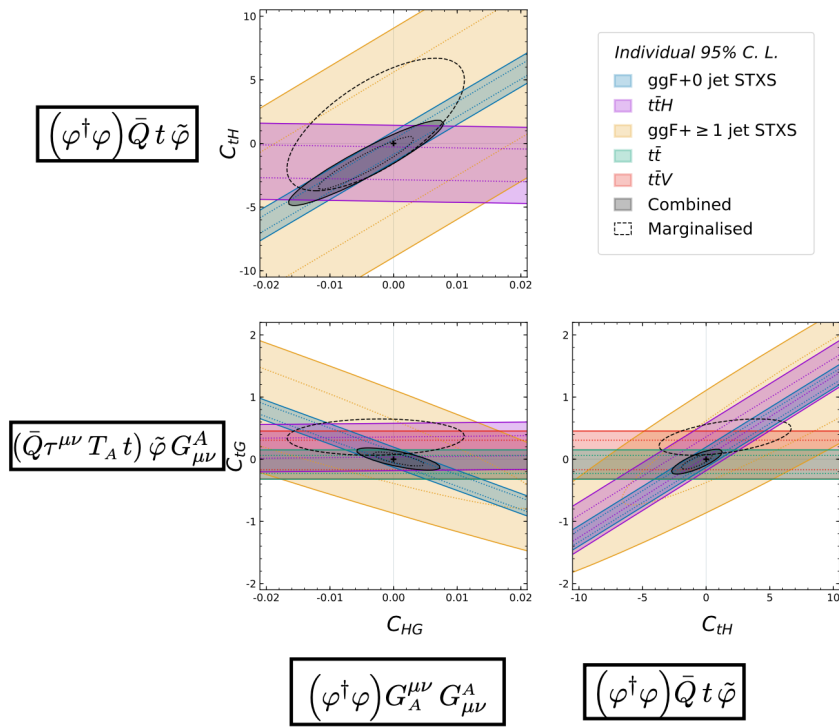


Figure 38: Figure from Ref. [28], shown at SM@LHC2021 by E.Vryonidou.

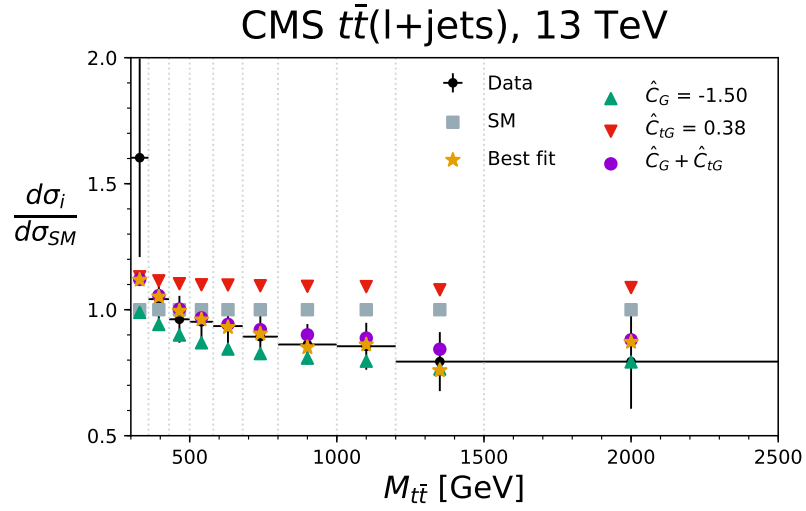


Figure 39: Invariant mass distribution of the $t\bar{t}$ pair measured by CMS compared to SM NNLO QCD+NLO EW predictions and fits to BSM interpretations. Figure from Ref. [28]

4 Higher orders in perturbation theory

4.1 Running coupling and scale dependence

In this section we would like to explain how it arises that theoretical predictions depend in general on at least one unphysical scale, the so-called *renormalisation scale* μ . In the case of hadronic initial state particles, there is also a *factorisation scale* μ_f involved. There can be even more unphysical scales, like fragmentation scales in the modelling of the fragmentation of final state particles into hadrons, parton shower matching scales, resummation scales, etc.

Let us first motivate how the dependence on a renormalisation scale arises. We mentioned already that the strong coupling, defined as $\alpha_s = g_s^2/(4\pi)$, is not really a constant. To leading order in the perturbative expansion, it obeys the relation

$$\alpha_s(Q^2) = \frac{1}{b_0 \log(Q^2/\Lambda_{QCD}^2)}, \quad (82)$$

where Λ_{QCD} is an energy scale below which non-perturbative effects start to dominate (the scale of bound states formation (hadrons)), and Q^2 is a larger energy scale, for example the centre-of-mass energy s of a scattering process. The coefficient b_0 is given by

$$b_0 = \frac{1}{4\pi} \left(\frac{11}{3} C_A - \frac{4}{3} T_R N_f \right). \quad (83)$$

Note that $b_0 > 0$ for $N_f < 11/2 C_A$.

Where does the running of the coupling come from? It is closely linked to renormalisation, which introduces the *renormalisation scale* μ .

Before we enter into the technicalities, let us look at a physical observable, for example the R -ratio which we encountered already,

$$R(s) = \frac{\sigma(e^+e^- \rightarrow \text{hadrons})}{\sigma(e^+e^- \rightarrow \mu^+\mu^-)}. \quad (84)$$

We assume that the energy s exchanged in the scattering process is much larger than Λ_{QCD} .

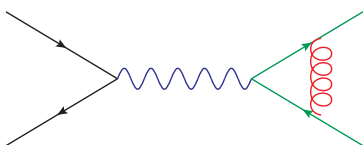
At leading order in perturbation theory, we have to calculate tree-level diagrams for $e^+e^- \rightarrow f\bar{f}$, which however only represent a crude approximation. To get a more precise result, we should include quantum corrections, for

example diagrams where virtual gluons are exchanged, such as the ones in Figs. 40a and 40b, where Fig. 40a shows corrections of order α_s and Fig. 40b shows example diagrams for $\mathcal{O}(\alpha_s^2)$ corrections. The perturbative expansion for R can be written as

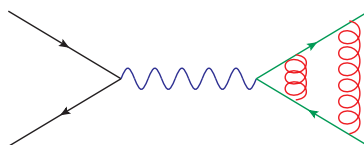
$$R(s) = K_{QCD}(s) R_0, \quad R_0 = N_c \sum_f Q_f^2 \theta(s - 4m_f^2),$$

$$K_{QCD}(s) = 1 + \frac{\alpha_s(\mu^2)}{\pi} + \sum_{n \geq 2} C_n \left(\frac{s}{\mu^2} \right) \left(\frac{\alpha_s(\mu^2)}{\pi} \right)^n. \quad (85)$$

The higher the order in α_s the harder is the calculation. Meanwhile we know the C_n up to order α_s^4 [29, 30].



(a) 1-loop diagram contributing to $e^+e^- \rightarrow f\bar{f}$.



(b) 2-loop diagram example contributing to $e^+e^- \rightarrow f\bar{f}$.

However, if we try to calculate the loop diagrams, we will realize that some of the integrals over the loop momentum k are ill-defined. They diverge for $k \rightarrow \infty$. This is called an *ultraviolet divergence*. How to deal with them will be explained shortly. For the moment we just introduce an arbitrary cutoff scale Λ_{UV} for the upper integration boundary. If we carried through the calculation, we would see that the dependence on the cutoff in diagram 40a cancels, which is a consequence of the Ward Identity in QED. However, if we go one order higher in α_s , calculating diagrams like the one in Fig. 40b, the cutoff-dependence does not cancel anymore. We obtain

$$K_{QCD}(s) = 1 + \frac{\alpha_s}{\pi} + \left(\frac{\alpha_s}{\pi} \right)^2 \left[c + b_0 \pi \log \frac{\Lambda_{UV}^2}{s} \right] + \mathcal{O}(\alpha_s^3). \quad (86)$$

It looks like our result is infinite, as we should take the limit $\Lambda_{UV} \rightarrow \infty$. However, we did not claim that α_s is the coupling we measure. In fact, it is the “bare” coupling, also denoted as α_s^0 , which appears in Eq. (86), and we can absorb the infinity in the bare coupling to arrive at the renormalised coupling, which is the one we measure.

In our case, this looks as follows. Define

$$\alpha_s(\mu) = \alpha_s^0 + b_0 \log \frac{\Lambda_{UV}^2}{\mu^2} \alpha_s^2, \quad (87)$$

then replace α_s^0 by $\alpha_s(\mu)$ and drop consistently all terms of order α_s^3 . This leads to

$$K_{QCD}^{\text{ren}}(\alpha_s(\mu), \mu^2/s) = 1 + \frac{\alpha_s(\mu)}{\pi} + \left(\frac{\alpha_s(\mu)}{\pi} \right)^2 \left[c + b_0 \pi \log \frac{\mu^2}{s} \right] + \mathcal{O}(\alpha_s^3). \quad (88)$$

K_{QCD}^{ren} is finite, but now it depends on the scale μ , both explicitly and through $\alpha_s(\mu)$. However, the hadronic R -ratio is a physical quantity and therefore cannot depend on the arbitrary scale μ . The dependence of K_{QCD} on μ is an artefact of the truncation of the perturbative series after the order α_s^2 .

Renormalisation group and asymptotic freedom

Since the hadronic R -ratio $R^{\text{ren}} = R_0 K_{QCD}^{\text{ren}}$ cannot depend μ , we know

$$\mu^2 \frac{d}{d\mu^2} R^{\text{ren}}(\alpha_s(\mu), \mu^2/Q^2) = 0 = \left(\mu^2 \frac{\partial}{\partial \mu^2} + \mu^2 \frac{\partial \alpha_s}{\partial \mu^2} \frac{\partial}{\partial \alpha_s} \right) R^{\text{ren}}(\alpha_s(\mu), \mu^2/Q^2). \quad (89)$$

Equation (89) is called *renormalisation group equation (RGE)*. Introducing the abbreviations

$$t = \ln \frac{Q^2}{\mu^2}, \quad \beta(\alpha_s) = \mu^2 \frac{\partial \alpha_s}{\partial \mu^2}, \quad (90)$$

the RGE becomes

$$\left(-\frac{\partial}{\partial t} + \beta(\alpha_s) \frac{\partial}{\partial \alpha_s} \right) R = 0. \quad (91)$$

This first order partial differential equation can be solved by implicitly defining a function $\alpha_s(Q^2)$, the *running coupling*, by

$$t = \int_{\alpha_s}^{\alpha_s(Q^2)} \frac{dx}{\beta(x)}, \quad \text{with } \alpha_s \equiv \alpha_s(\mu^2). \quad (92)$$

Differentiating Eq. (92) with respect to the variable t leads to

$$1 = \frac{1}{\beta(\alpha_s(Q^2))} \frac{\partial \alpha_s(Q^2)}{\partial t}, \quad \text{which implies } \beta(\alpha_s(Q^2)) = \frac{\partial \alpha_s(Q^2)}{\partial t}.$$

The derivative of Eq. (92) with respect to α_s gives

$$0 = \frac{1}{\beta(\alpha_s(Q^2))} \frac{\partial \alpha_s(Q^2)}{\partial \alpha_s} - \frac{1}{\beta(\alpha_s)} \frac{\partial \alpha_s}{\partial \alpha_s} \Rightarrow \frac{\partial \alpha_s(Q^2)}{\partial \alpha_s} = \frac{\beta(\alpha_s(Q^2))}{\beta(\alpha_s)}. \quad (93)$$

It is now easy to prove that the value of R for $\mu^2 = Q^2$, $R(1, \alpha_s(Q^2))$, solves Eq. (91):

$$-\frac{\partial}{\partial t} R(1, \alpha_s(Q^2)) = -\frac{\partial R}{\partial \alpha_s(Q^2)} \frac{\partial \alpha_s(Q^2)}{\partial t} = -\beta(\alpha_s(Q^2)) \frac{\partial R}{\partial \alpha_s(Q^2)} \quad (94)$$

and

$$\beta(\alpha_s) \frac{\partial}{\partial \alpha_s} R(1, \alpha_s(Q^2)) = \beta(\alpha_s) \frac{\partial \alpha_s(Q^2)}{\partial \alpha_s} \frac{\partial R}{\partial \alpha_s(Q^2)} = \beta(\alpha_s(Q^2)) \frac{\partial R}{\partial \alpha_s(Q^2)}. \quad (95)$$

This means that the scale dependence in R enters only through $\alpha_s(Q^2)$, and that we can predict the scale dependence of R by solving Eq. (92), or equivalently,

$$\frac{\partial \alpha_s(Q^2)}{\partial t} = \beta(\alpha_s(Q^2)). \quad (96)$$

We can solve Eq. (96) perturbatively using an expansion of the β -function

$$\beta(\alpha_s) = -b_0 \alpha_s^2 \left[1 + \sum_{n=1}^{\infty} b_n \alpha_s^n \right], \quad (97)$$

where $b_0 = \frac{\beta_0}{4\pi}$ and $b_0 b_1 = \frac{\beta_1}{(4\pi)^2}$, etc. Explicitly, up to NNLO:

$$\mu^2 \frac{d\alpha_s(\mu)}{d\mu^2} = -\alpha_s(\mu) \left[\beta_0 \left(\frac{\alpha_s(\mu)}{2\pi} \right) + \beta_1 \left(\frac{\alpha_s(\mu)}{2\pi} \right)^2 + \beta_2 \left(\frac{\alpha_s(\mu)}{2\pi} \right)^3 + \mathcal{O}(\alpha_s^4) \right].$$

The first five coefficients are known [31], where the fifth one has been calculated only recently [32–36]. The first 3 coefficients ($\overline{\text{MS}}$ -scheme) are

$$\begin{aligned} \beta_0 &= \frac{11 C_A - 4 T_R N_F}{6}, \\ \beta_1 &= \frac{17 C_A^2 - 10 C_A T_R N_F - 6 C_F T_R N_F}{6}, \\ \beta_2 &= \frac{1}{432} (2857 C_A^3 + 108 C_F^2 T_R N_F - 1230 C_F C_A T_R N_F - 2830 C_A^2 T_R N_F \\ &\quad + 264 C_F T_R^2 N_F^2 + 316 C_A T_R^2 N_F^2). \end{aligned} \quad (98)$$

Introducing Λ as integration constant with $L = \log(\mu^2/\Lambda^2)$ yields the following solution up to order NNLO:

$$\alpha_s(\mu) = \frac{4\pi}{\beta_0 L} \left(1 - \frac{\beta_1}{\beta_0^2} \frac{\log L}{L} + \frac{1}{\beta_0^2 L^2} \left(\frac{\beta_1^2}{\beta_0^2} (\log^2 L - \log L - 1) + \frac{\beta_2}{\beta_0} \right) \right). \quad (99)$$

Truncating the series Eq. (97) at leading order leads to the simple solution Eq. (82), or, without introducing Λ ,

$$\begin{aligned} Q^2 \frac{\partial \alpha_s}{\partial Q^2} = \frac{\partial \alpha_s}{\partial t} = -b_0 \alpha_s^2 &\Rightarrow -\frac{1}{\alpha_s(Q^2)} + \frac{1}{\alpha_s(\mu^2)} = -b_0 t \\ \Rightarrow \alpha_s(Q^2) = \frac{\alpha_s(\mu^2)}{1 + b_0 t \alpha_s(\mu^2)}. \end{aligned} \quad (100)$$

Eq. (100) implies that

$$\alpha_s(Q^2) \xrightarrow{Q^2 \rightarrow \infty} \frac{1}{b_0 t} \xrightarrow{Q^2 \rightarrow \infty} 0. \quad (101)$$

This behaviour is called *asymptotic freedom*: the larger Q^2 , the smaller the coupling, so at very high energies (small distances), the quarks and gluons can be treated as if they were free particles. The behaviour of α_s as a function

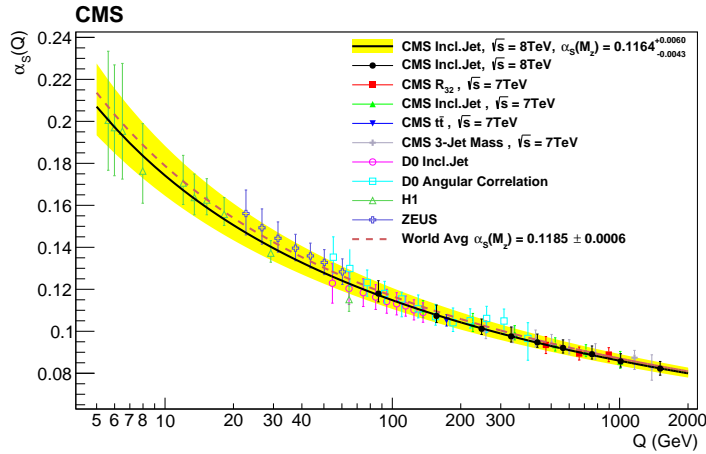


Figure 41: The running coupling $\alpha_s(Q^2)$. *Figure from arXiv:1609.05331.*

of Q^2 is illustrated in Fig. 41 including recent measurements. Note that the

sign of b_0 is positive for QCD, while it is negative for QED. It can be proven that, in 4 space-time dimensions, only non-Abelian gauge theories can be asymptotically free. For the discovery of asymptotic freedom in QCD [37,38], Gross, Politzer and Wilczek got the Nobel Prize in 2004.

Note that in the derivation of the RGE above, we have assumed that the observable R does not depend on other mass scales like quark masses. However, the renormalisation group equations can be easily extended to include mass renormalisation, which will lead to running quark masses:

$$\left(\mu^2 \frac{\partial}{\partial \mu^2} + \beta(\alpha_s) \frac{\partial}{\partial \alpha_s} - \gamma_m(\alpha_s) m \frac{\partial}{\partial m} \right) R \left(\frac{Q^2}{\mu^2}, \alpha_s, \frac{m}{Q} \right) = 0, \quad (102)$$

where γ_m is called the *mass anomalous dimension* and the minus sign before γ_m is a convention. In a perturbative expansion we can write the mass anomalous dimension as $\gamma_m(\alpha_s) = c_0 \alpha_s (1 + \sum_n c_n \alpha_s^n)$. The coefficients are known up to c_4 [39–42].

Scale uncertainties

From the perturbative solution of the RGE we can derive how a physical quantity $O^{(N)}(\mu)$, expanded in α_s as $O^{(N)}(\mu) = \sum_{n=0}^N C_n(\mu) \alpha_s^{n+k}(\mu^2)$ and truncated at order N in perturbation theory (k is the power of α_s at leading order), changes with the renormalisation scale μ :

$$\frac{d}{d \log(\mu^2)} O^{(N)}(\mu) \sim \mathcal{O}(\alpha_s(\mu^2)^{N+1}). \quad (103)$$

Therefore it is clear that, the more higher order coefficients c_n we can calculate, the less our result will depend on the unphysical scale μ^2 . Therefore the dependence of the scale is used to estimate the uncertainty of a result calculated to a certain order in perturbation theory. Usually the scale is varied by a factor of two up and down. An example for the reduction of the scale dependence at higher orders is shown in Fig. 42.

An expansion up to NNLO of an observable O normalised to the LO cross section σ_0 can be written as

$$\frac{1}{\sigma_0} \frac{d\sigma}{dO} = \left(\frac{\alpha_s}{2\pi} \right) \frac{dC_1}{dO} + \left(\frac{\alpha_s}{2\pi} \right)^2 \frac{dC_2}{dO} + \left(\frac{\alpha_s}{2\pi} \right)^3 \frac{dC_3}{dO} + \mathcal{O}(\alpha_s^4). \quad (104)$$

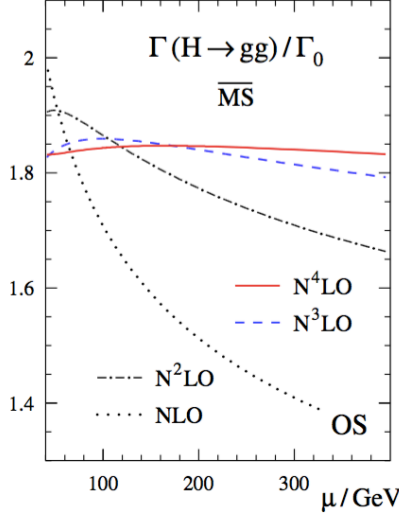


Figure 42: Example $H \rightarrow gg$ for the reduction of the scale dependence at higher orders. *Figure from Ref. [30], see also [36].*

In terms of the running coupling $\alpha_s(\mu)$, the NNLO expression becomes

$$\begin{aligned}
\frac{1}{\sigma_0} \frac{d\sigma}{dO}(s, \mu^2, O) = & \\
& \left(\frac{\alpha_s(\mu)}{2\pi} \right) \frac{dC_1}{dO} + \left(\frac{\alpha_s(\mu)}{2\pi} \right)^2 \left(\frac{dC_2}{dO} + \frac{dC_1}{dO} \beta_0 \log \frac{\mu^2}{s} \right) \\
& + \left(\frac{\alpha_s(\mu)}{2\pi} \right)^3 \left(\frac{dC_3}{dO} + 2 \frac{dC_2}{dO} \beta_0 \log \frac{\mu^2}{s} + \frac{dC_1}{dO} \left(\beta_0^2 \log^2 \frac{\mu^2}{s} + \beta_1 \log \frac{\mu^2}{s} \right) \right) \\
& + \mathcal{O}(\alpha_s^4). \tag{105}
\end{aligned}$$

As an example we consider an observable called *thrust*, shown in Fig. 43. Thrust is an example of so-called *event-shape* observables, which describes how “pencil-like” an event looks like. Events shapes can be defined based on hadronic tracks in the detector, avoiding jet definitions, and are particularly useful in e^+e^- annihilation, where the total energy of the partonic event is known. Thrust T is defined by

$$T = \max_{\vec{n}} \frac{\sum_{i=1}^m |\vec{p}_i \cdot \vec{n}|}{\sum_{i=1}^m |\vec{p}_i|}, \tag{106}$$

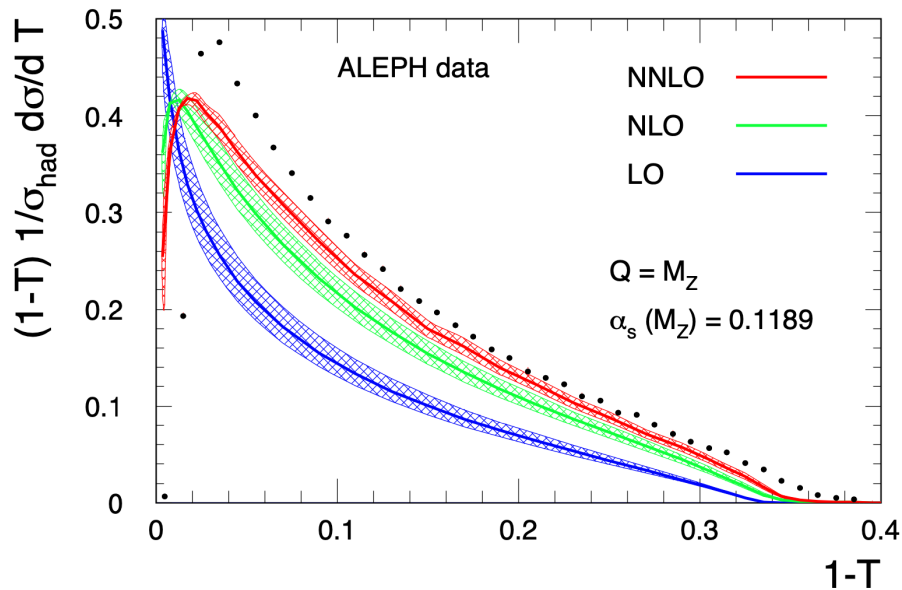


Figure 43: One minus thrust distribution at different orders in perturbation theory, including scale uncertainty bands. *Figure from Ref. [43].*

where \vec{n} is a three-vector (the direction of the thrust axis) such that T is maximal. The particle three-momenta \vec{p}_i are defined in the e^+e^- centre-of-mass frame.

Fig. 43 shows several features: 1. the scale dependence is reduced as the perturbative order increases, 2. the NNLO curve is closest to the data, 3. the data are still not well described by NNLO. The reasons for the latter are well understood: The perturbative prediction for the thrust distribution becomes singular as $T \rightarrow 1$, there is also a logarithmic divergence $\sim \ln(1-T)$. The latter is characteristic for events shape distributions. In perturbation theory at n th order logarithms of the form $\alpha_s^n \ln^m(1/(1-T))$ with $m \leq 2n$ appear. These spoil the convergence of the perturbative series and should be “resummed” if we want to make reliable prediction near the phase space region where $T \rightarrow 1$. Furthermore, the so-called *power corrections*, the terms of $\mathcal{O}\left(\frac{\Lambda}{Q}\right)^p$ in Eq. (2), play a role for this observable.

In hadronic collisions there is another scale, the factorisation scale μ_f , which needs to be taken into account when assessing the uncertainty of the theoretic-

cal prediction. Varying both μ_r and μ_f simultaneously in the same directions can lead to accidental cancellations and hence underestimation of the perturbative uncertainties. Therefore, in the presence of both μ_r and μ_f , often so-called *7-point scale variations* are performed, which means $\mu_{r,f} = c_{r,f}\mu_0$, where $c_r, c_f \in \{2, 1, 0.5\}$ and where the extreme variations $(c_r, c_f) = (2, 0.5)$ and $(c_r, c_f) = (0.5, 2)$ have been omitted.

Still, the question remains what to choose for the central scale μ_0 . A convenient choice is a scale where the higher order corrections are small, i.e. a scale showing good “perturbative stability”. In Fig. 42, a good choice would be $\mu_0 \approx 150$ GeV.

Let us now see a few examples where such scale variations do not capture the true uncertainties. First some preliminary remarks, along the lines of Ref. [44]. If there is only one scale μ_r involved, the the scale dependence of an observable is given through $\alpha_s(\mu_r)$, and we can use the beta-function, resp. Eq. (99), to move from a result at a scale μ_0 to a result at a different scale. For an observable O , known to order α_s^N ,

$$O = \sum_{n=0}^N C_n(\mu_r) \alpha_s^{n+k}(\mu_r);,$$

where k is the power of α_s at leading order, we therefore have (this time not normalised to the LO cross section)

$$O = C_0 \alpha_s^k(\mu_r) + \left(C_1 + b_0 C_0 \ln \left(\frac{\mu_r^2}{\mu_0^2} \right) \right) \alpha_s^{k+1}(\mu_r) + \mathcal{O}(\alpha_s^{k+2}). \quad (107)$$

Variations of μ_r will change the C_0 -part of the $\mathcal{O}(\alpha_s^{k+2})$ term, however the magnitude of C_1 can only be known by direct calculation.

To illustrate the improvement in scale uncertainty that may occur at NNLO, let us consider the corrections up to (N)NLO for an observable as for example a jet cross section as a function of transverse energy, where $k = 2$. The renormalisation scale dependence is entirely predictable,

$$\begin{aligned} \frac{d\sigma}{dE_T} &= \alpha_s^2(\mu_r) C_0 \\ &+ \alpha_s^3(\mu_r) (C_1 + 2b_0 L C_0) \\ &+ \alpha_s^4(\mu_r) (C_2 + 3b_0 L C_1 + (3b_0^2 L^2 + 2b_1 L) C_0) \end{aligned} \quad (108)$$

with $L = \ln(\mu_r/E_T)$. C_0 and C_1 are the known LO and NLO coefficients. Now assume that C_2 is an unknown NNLO term (note however that C_2 is known meanwhile [45, 46]). Fig. 44 shows that the scale dependence is systematically reduced by increasing the number of terms in the perturbative expansion. At NLO, there is always a turning point where the prediction is insensitive to small changes in μ_r . If this occurs at a scale far from the typically chosen values of μ_r , the NLO K -factor (defined as $K = 1 + \alpha_s(\mu_r)C_1/C_0$) will be large. At NNLO the scale dependence is clearly significantly reduced. However, a more quantitative statement requires knowledge of C_2 .

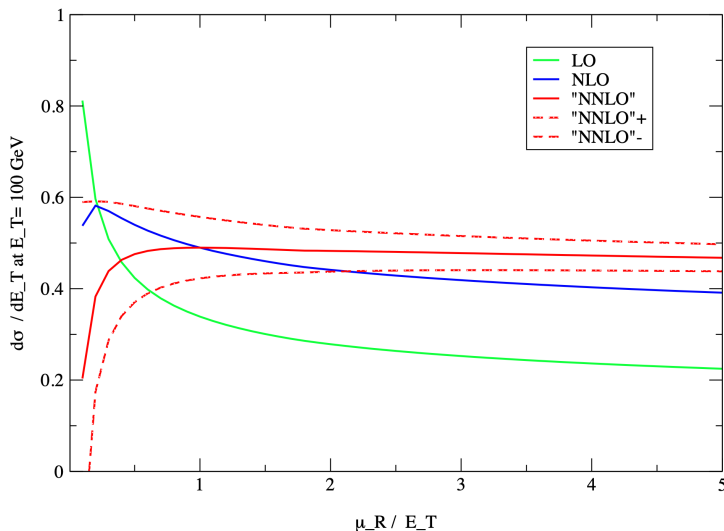


Figure 44: Single jet inclusive distribution at $E_T = 100$ GeV and $0.1 < |\eta| < 0.7$ at $\sqrt{s} = 1800$ GeV at LO (green), NLO (blue) and NNLO (red). The solid and dashed red lines show the NNLO prediction if $C_2 = 0$, $C_2 = \pm C_1^2/C_0$ respectively. Figure from Ref. [44].

For some processes, C_1 (and C_2) turned out to be pretty large, and the scale uncertainty bands obtained from 7-point scale variations do not (fully) overlap between the different orders. One such example is Higgs production in gluon fusion, known to order N^3LO . Fig. 45 shows a very nice stabilisation of the scale dependence, however the higher order corrections are very large. The standard scale uncertainty bands are shown in Fig. 46. Among the reasons for the large K -factors, in particular the NLO K -factor, are large colour factors and new partonic channels opening up.

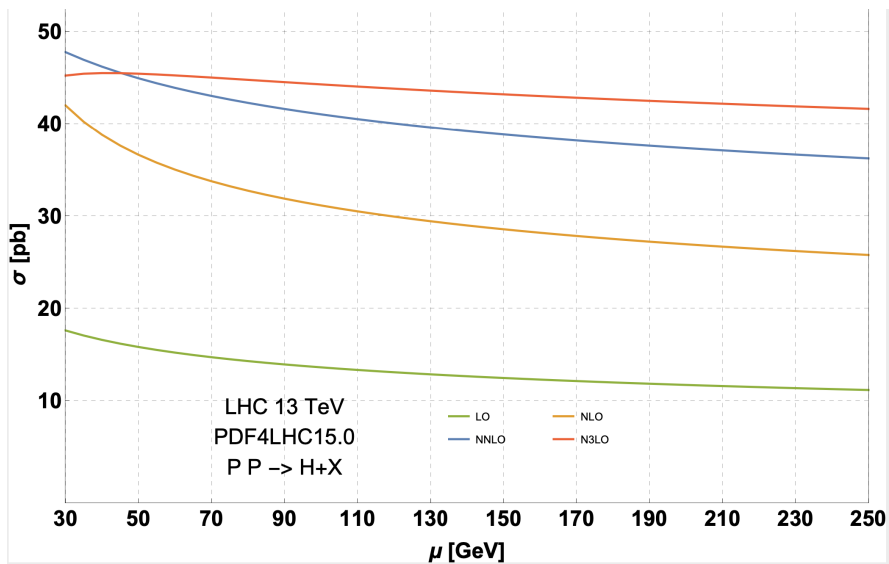


Figure 45: Higgs production in gluon fusion, stabilisation of the scale dependence. Figure from Ref. [47].

In Fig. 47 the μ_f and μ_r dependence is shown separately. Usually one can see that the perturbative series stabilises at latest between NNLO and N3LO. However, for charged current Drell-Yan production and a central scale of $Q = 100$ GeV, shown in Fig. 48, the NNLO and N3LO uncertainty bands do not overlap.

Looking at the μ_f dependence separately, one can see that the NNLO band is accidentally small, see Fig. 49.

Furthermore, the behaviour of the scale uncertainty bands can depend sensitively on the definition of the central μ , see Fig. 50. The different central scale choices are

- the individual jet transverse momentum p_T . This however can lead to the scale being set to values that are not representative of the scale of the underlying hard scattering process.
- The leading-jet transverse momentum $p_{T,1}$, This scale uses the transverse momentum of the hardest jet in the event, which is a better proxy for the scale of the hard interaction compared to the $\mu = p_T$ choice.
- The scalar sum of the transverse momenta of all reconstructed jets H_T , $H_T = \sum_{i \in \text{jets}} p_{T,i}$.

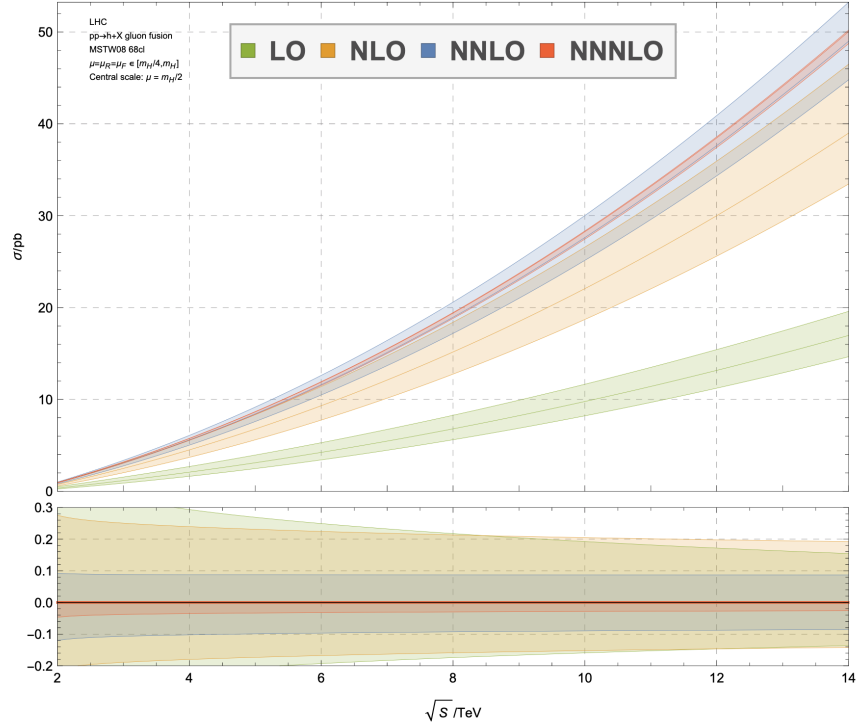


Figure 46: Scale uncertainty bands for Higgs production in gluon fusion. Figure from Ref. [48].

- The scalar sum of the transverse momenta of all partons \hat{H}_T : the transverse momentum sum is not based on the reconstructed jets, but instead obtained as the transverse momentum sum of all partons in the event: $\hat{H}_T = \sum_{i \in \text{partons}} p_{T,i}$. This scale choice also has the advantage of being insensitive to the jet reconstruction applied in the analysis and is an infrared-safe event shape variable.

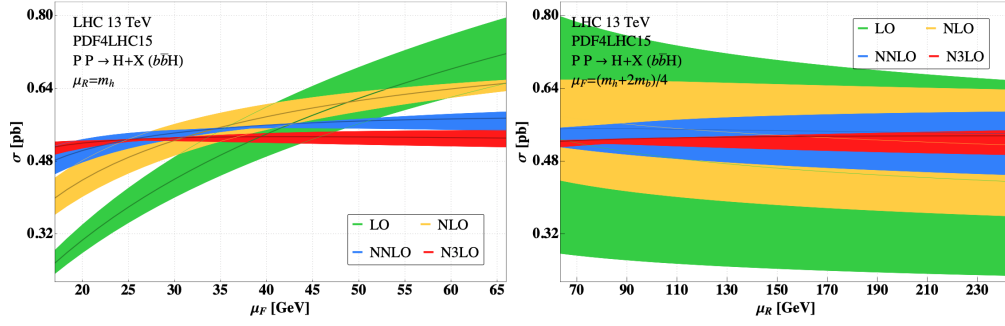


Figure 47: Higgs production in bottom quark fusion. Figure from Ref. [49].

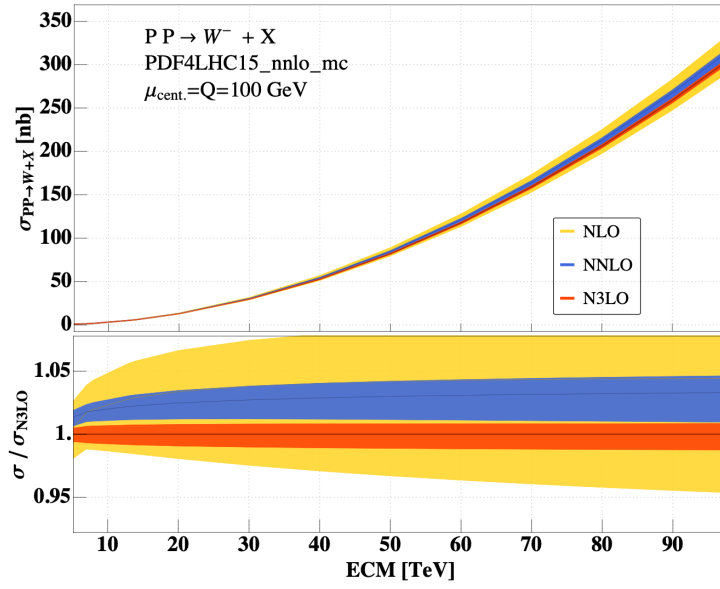


Figure 48: Charged current Drell-Yan production, $pp \rightarrow W^-$. Figure from Ref. [50].

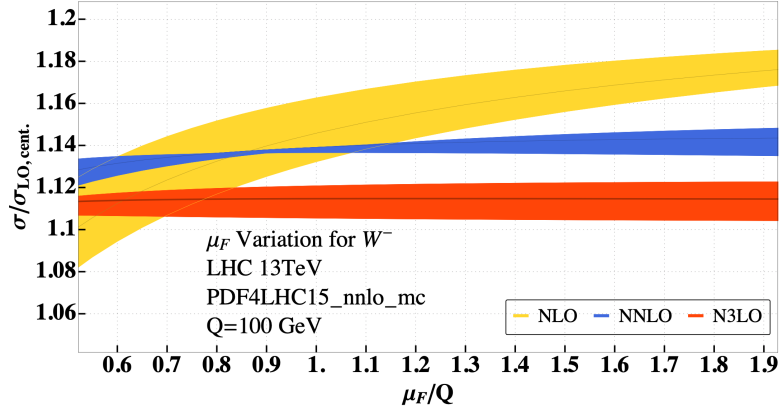


Figure 49: Charged current Drell-Yan production, μ_f -dependence. Figure from Ref. [50].

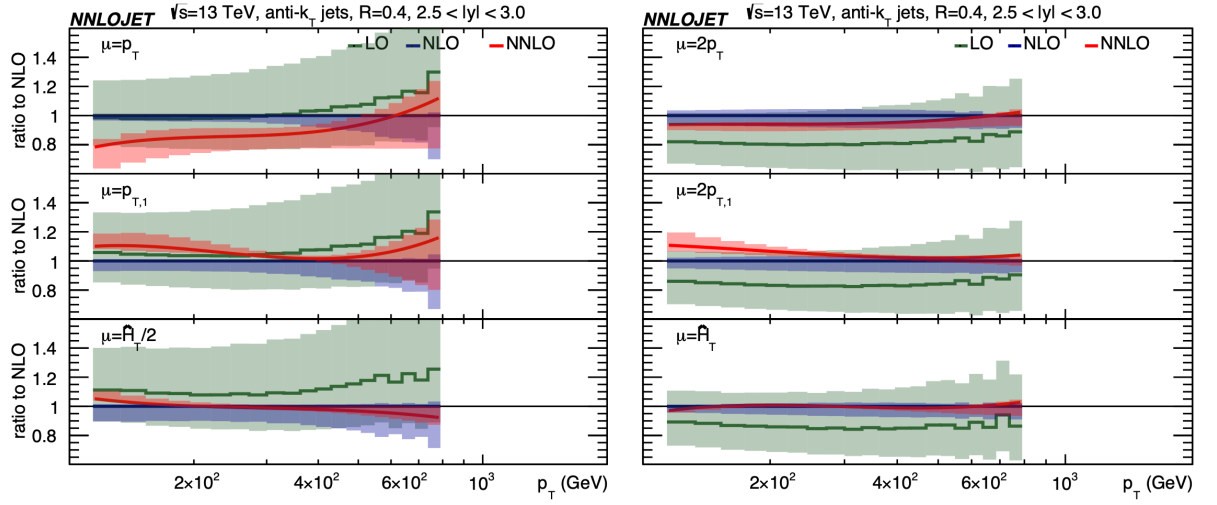


Figure 50: Inclusive jet p_T spectrum integrated over rapidity at LO (green), NLO (blue) and NNLO (red) normalised to the NLO prediction as a function of the central scale choice for cone size $R = 0.4$. Figure from Ref. [51].

4.2 Loops and divergences

4.3 Dimensional regularisation

Tree level results in QCD are mostly not accurate enough to match the current experimental precision and suffer from large scale uncertainties. When calculating higher orders, we encounter singularities: ultraviolet (UV) singularities, and infrared (IR) singularities due to soft or collinear massless particles. Therefore the introduction of a *regulator* is necessary.

Let us first have a look at UV singularities: The expression for the one-loop two-point function shown below naively would be

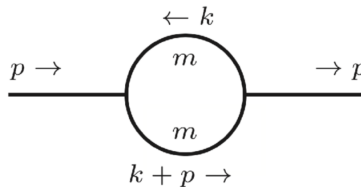


Figure 51: One-loop two-point function (“bubble”).

$$I_2 = \int_{-\infty}^{\infty} \frac{d^4k}{(2\pi)^4} \frac{1}{[k^2 - m^2 + i\delta][(k+p)^2 - m^2 + i\delta]} . \quad (109)$$

If we are only interested in the behaviour of the integral for $|k| \rightarrow \infty$ we can neglect the masses, transform to polar coordinates and obtain

$$I_2 \sim \int d\Omega_3 \int_0^{\infty} d|k| \frac{|k|^3}{|k|^4} . \quad (110)$$

This integral is clearly not well-defined. If we introduce an upper cutoff Λ (and a lower limit $|k|_{\min}$ because we neglected the masses and p^2 , which would serve as an IR regulator), it is regulated:

$$I_2 \sim \int_{|k|_{\min}}^{\Lambda} d|k| \frac{1}{|k|} \sim \log \left(\frac{\Lambda}{|k|_{\min}} \right) . \quad (111)$$

The integral has a logarithmic UV divergence for $\Lambda \rightarrow \infty$. The problem with cut-off regularisation with a regulator Λ is that it is neither a Lorentz invariant nor a gauge invariant way to regulate integrals over loop momenta.

A regularisation method which preserves the symmetries is *dimensional regularisation*.

Dimensional regularisation has been introduced in 1972 by 't Hooft and Veltman [52] (and by Bollini and Giambiagi [53]) as a method to regularise UV divergences in a gauge invariant way, thus completing the proof of renormalisability.

The idea is to work in $D = 4 - 2\epsilon$ space-time dimensions. Divergences for $D \rightarrow 4$ will appear as poles in $1/\epsilon$. This means that the Lorentz algebra objects (momenta, polarisation vectors, metric tensor) live in a D -dimensional space. The γ -algebra also has to be extended to D dimensions. How to treat internal and external Lorentz vectors and the γ -algebra is not unique. There are several *regularisation schemes* within dimensional regularisation. For example, when doing a calculation in supersymmetry, you may not want to use a scheme where massless bosons have $D - 2$ polarisation states while massless fermions have 2 polarisation states. Of course the different schemes must lead to the same result for physical quantities.

An important feature of dimensional regularisation is that it regulates IR singularities, i.e. divergences occurring when massless particles become soft and/or collinear, as well. Ultraviolet divergences occur for loop momenta $k \rightarrow \infty$, so in general the UV behaviour becomes better for $\epsilon > 0$, while the IR behaviour becomes better for $\epsilon < 0$. Certainly we cannot have $D < 4$ and $D > 4$ at the same time. What is formally done is to first assume the IR divergences are regulated in some other way, e.g. by assuming all external legs are off-shell or by introducing a small mass for all massless particles. In this case all poles in $1/\epsilon$ will be of UV nature and renormalisation can be performed. Then we can analytically continue to the whole complex D -plane, in particular to $\text{Re}(D) > 4$. If we now remove the auxiliary IR regulator, the IR divergences will show up as $1/\epsilon$ poles. (This is however not done in practice, where all poles just show up as $1/\epsilon$ poles, and after UV renormalisation, the remaining poles must be of IR nature.)

Naive degree of divergence

The naive degree of UV divergence ω of an integral can be determined by power counting: if we work in D dimensions at L loops, and consider an integral with P propagators and n_l factors of the loop momentum belonging to loop $l \in \{1, \dots, L\}$ in the numerator, we have $\omega = D L - 2P + 2 \sum_l \lfloor n_l/2 \rfloor$, where $\lfloor n_l/2 \rfloor$ is the nearest integer less or equal to $n_l/2$. We have logarithmic

mic, linear, quadratic, ... overall divergences for $\omega = 0, 1, 2, \dots$ and no UV divergence for $\omega < 0$. This means that in 4 dimensions at one loop, we have UV divergences in all two-point functions, three-point functions with rank ≥ 2 and four-point functions with rank ≥ 4 .

These considerations do not take into account UV subdivergences of multi-loop integrals, or a reduction of the degree of divergence due to gauge cancellations. Therefore ω is called *naive* or *superficial* degree of divergence.

In dimensional regularisation, the only change to the Feynman rules to be made is to multiply the couplings in the Lagrangian by a factor μ^ϵ : $g \rightarrow g\mu^\epsilon$, where μ is an arbitrary mass scale. This ensures that each term in the Lagrangian has the correct mass dimension. The momentum integration involves $\int \frac{d^D k}{(2\pi)^D}$ for each loop.

4.4 One-loop integrals

Integration in D dimensions

We first consider a scalar one-loop diagram with N external legs and N propagators, as given in (112). The case with loop momenta in the numerator (“tensor integrals”) will be treated later. If k is the loop momentum, the momenta of the propagators are $q_a = k + r_a$, where $r_a = \sum_{i=1}^a p_i$. If we define all momenta as incoming, momentum conservation implies $\sum_{i=1}^N p_i = 0$ and hence $r_N = 0$.

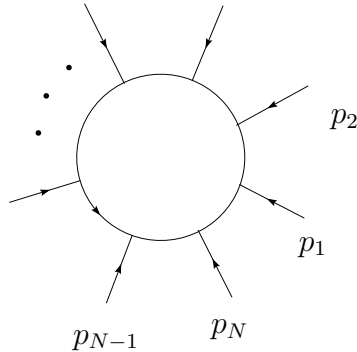


Figure 52: Generic one-loop integral

$$I_N^D = \int_{-\infty}^{\infty} \frac{d^D k}{i\pi^{\frac{D}{2}}} \frac{1}{\prod_{i=1}^N (q_i^2 - m_i^2 + i\delta)}. \quad (112)$$

We use the integration measure $d^D k / i\pi^{\frac{D}{2}} \equiv d\kappa$ to avoid ubiquitous factors of $i\pi^{\frac{D}{2}}$ which will arise upon momentum integration.

Feynman parameters

To combine products of denominators of the type $d_i^{n_i} = [(k+r_i)^2 - m_i^2 + i\delta]^{n_i}$ into one single denominator, we can use the identity

$$\frac{1}{d_1^{n_1} d_2^{n_2} \dots d_N^{n_N}} = \frac{\Gamma(\sum_{i=1}^N n_i)}{\prod_{i=1}^N \Gamma(n_i)} \int_0^\infty \prod_{i=1}^N dz_i z_i^{n_i-1} \frac{\delta(1 - \sum_{j=1}^N z_j)}{[z_1 d_1 + z_2 d_2 + \dots + z_N d_N]^{\sum_{i=1}^N n_i}} \quad (113)$$

The integration parameters z_i are called *Feynman parameters*. For generic one-loop diagrams we have $n_i = 1 \forall i$. Propagator powers n_i different from one become important when we derive relations between integrals.

Schwinger parametrisation

An alternative to Feynman parametrisation is the so-called ‘‘Schwinger parametrisation’’, based on

$$\frac{1}{d_i^{n_i}} = \frac{1}{\Gamma(n_i)} \int_0^\infty d\alpha \alpha^{n_i-1} \exp(-\alpha d_i), \quad \text{Re}(d_i) > 0, \quad (114)$$

which can be derived from the definition of the Γ -function

$$\Gamma(t) = \int_0^\infty dx x^{t-1} \exp(-x), \quad \text{Re}(t) > 0. \quad (115)$$

The Gaussian integration formula

$$\int_{-\infty}^{\infty} d^D r_E \exp(-\alpha r_E^2) = \left(\frac{\pi}{\alpha}\right)^{\frac{D}{2}}, \quad \alpha > 0 \quad (116)$$

can be used to integrate over the momenta (after Wick rotation) in the Schwinger parametrisation.

Simple example: one-loop two-point function

For $N = 2$, (2-point integral), the Feynman parametrisation is given by

$$\begin{aligned}
I_2 &= \int_{-\infty}^{\infty} d\kappa \frac{1}{[k^2 - m^2 + i\delta][(k+p)^2 - m^2 + i\delta]} \\
&= \Gamma(2) \int_0^{\infty} dz_1 dz_2 \int_{-\infty}^{\infty} d\kappa \frac{\delta(1 - z_1 - z_2)}{[z_1(k^2 - m^2) + z_2((k+p)^2 - m^2) + i\delta]^2} \\
&= \int_0^1 dx \int_{-\infty}^{\infty} d\kappa \frac{1}{[k^2 + 2xk \cdot p + xp^2 - m^2 + i\delta]^2}, \tag{117}
\end{aligned}$$

where we have substituted $z_1 = (1-x)u$, $z_2 = x$ before the last line. As the momentum integral is shift invariant, we can substitute $l = k + xp$ to eliminate the term linear in the loop momentum, to arrive at

$$I_2 = \int_0^1 dx \int_{-\infty}^{\infty} \frac{d^D l}{i\pi^{\frac{D}{2}}} \frac{1}{[l^2 + p^2 x(1-x) - m^2 + i\delta]^2}. \tag{118}$$

For integrals with more external legs the linear term can be eliminated by an analogous shift of the loop momentum. Therefore, the generic form of a one-loop integral after Feynman parametrisation and after having performed the shift to achieve a quadratic form in the loop momentum is given by

$$I_N^D = \Gamma(N) \int_0^{\infty} \prod_{i=1}^N dz_i \delta(1 - \sum_{j=1}^N z_j) \int_{-\infty}^{\infty} \frac{d^D l}{i\pi^{\frac{D}{2}}} [l^2 - R^2 + i\delta]^{-N} \tag{119}$$

where for $N = 2$ and both propagators massive we have just derived $R = -p^2 x(1-x) + m^2$.

For the general case, one finds

$$R^2 = -\frac{1}{2} \sum_{i,j=1}^N z_i z_j \mathcal{S}_{ij} \quad \text{with} \tag{120}$$

$$\mathcal{S}_{ij} = (r_i - r_j)^2 - m_i^2 - m_j^2, \quad \sum_{i=1}^N z_i = 1. \tag{121}$$

The matrix \mathcal{S}_{ij} , sometimes also called *Cayley matrix*, is the quantity encoding all the kinematic dependence of the integral. It plays a major role in the algebraic reduction of tensor integrals or integrals with higher N to simpler objects, as well as in the analysis of the kinematic singularities of the integrand.

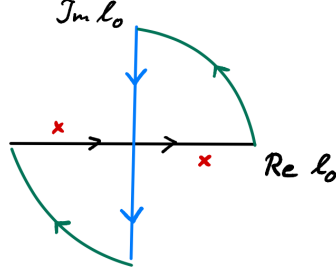


Figure 53: Integration contour after Wick rotation.

Momentum integration for scalar one-loop N-point integrals

Now we perform the momentum integration for an integral of the form Eq. (119). Remember that we are in Minkowski space, where $l^2 = l_0^2 - \vec{l}^2$, so temporal and spatial components are not on equal footing. The poles of the denominator in Eq. (119) are located at $l_0^2 = R^2 + \vec{l}^2 - i\delta \Rightarrow l_0^\pm \simeq \pm\sqrt{R^2 + \vec{l}^2} \mp i\delta$. Thus the $i\delta$ term shifts the poles away from the real axis in the l_0 -plane.

For the integration over the loop momentum, we better work in Euclidean space where $l_E^2 = \sum_{i=1}^D l_i^2$. Hence we make the transformation $l_0 \rightarrow il_4$, such that $l^2 \rightarrow -l_E^2 = l_4^2 + \vec{l}^2$, which implies that the integration contour in the complex l_0 -plane is rotated by 90° such that the contour in the complex l_4 -plane looks as shown below. This is called *Wick rotation*. We see that the $i\delta$ prescription is exactly such that the contour does not enclose any poles. Therefore the integral over the closed contour is zero, and we can use the identity

$$\int_{-\infty}^{\infty} dl_0 f(l_0) = i \int_{-\infty}^{\infty} dl_4 f(l_4) \quad (122)$$

Our integral now reads

$$I_N^D = (-1)^N \Gamma(N) \int_0^\infty \prod_{i=1}^N dz_i \delta\left(1 - \sum_{l=1}^N z_l\right) \int_{-\infty}^{\infty} \frac{d^D l_E}{\pi^{\frac{D}{2}}} [l_E^2 + R^2 - i\delta]^{-N} \quad (123)$$

Now we can introduce polar coordinates in D dimensions to evaluate the

momentum integral.

$$\int_{-\infty}^{\infty} d^D l_E = \int_0^{\infty} dr r^{D-1} \int d\Omega_{D-1}, \quad r = \sqrt{l_E^2} = \left(\sum_{i=1}^4 l_i^2 \right)^{\frac{1}{2}} \quad (124)$$

$$\int d\Omega_{D-1} = V(D) = \frac{2\pi^{\frac{D}{2}}}{\Gamma(\frac{D}{2})} \quad (125)$$

where $V(D)$ is the volume of a unit sphere in D dimensions, which we encountered already in the context of D -dimensional phase space integrals. Thus we have

$$I_N^D = 2(-1)^N \frac{\Gamma(N)}{\Gamma(\frac{D}{2})} \int_0^{\infty} \prod_{i=1}^N dz_i \delta(1 - \sum_{l=1}^N z_l) \int_0^{\infty} dr r^{D-1} \frac{1}{[r^2 + R^2 - i\delta]^N}$$

Substituting $r^2 = x$:

$$\int_0^{\infty} dr r^{D-1} \frac{1}{[r^2 + R^2 - i\delta]^N} = \frac{1}{2} \int_0^{\infty} dx x^{D/2-1} \frac{1}{[x + R^2 - i\delta]^N} \quad (126)$$

Now the substitution $x = zR^2$ can be done to arrive at

$$\frac{1}{2} \int_0^{\infty} dx x^{D/2-1} \frac{1}{[x + R^2 - i\delta]^N} = \frac{1}{2} [R^2 - i\delta]^{\frac{D}{2}-N} \int_0^{\infty} dz z^{D/2-1} [1 + z]^{-N}. \quad (127)$$

Note that we still carry along the $-i\delta$ term because it can be useful to indicate the direction of the analytic continuation when performing the integrals over the Feynman parameters. As it only indicates an infinitesimal shift, we can always rescale δ by a positive quantity. The z -integral can be identified as the Euler Beta-function $B(a, b)$, defined as

$$B(a, b) = \int_0^{\infty} dz \frac{z^{a-1}}{(1+z)^{a+b}} = \int_0^1 dy y^{a-1} (1-y)^{b-1} = \frac{\Gamma(a)\Gamma(b)}{\Gamma(a+b)}, \quad (128)$$

to finally arrive at

$$I_N^D = (-1)^N \Gamma(N - \frac{D}{2}) \int_0^{\infty} \prod_{i=1}^N dz_i \delta(1 - \sum_{l=1}^N z_l) [R^2 - i\delta]^{\frac{D}{2}-N} \quad (129)$$

The integration over the Feynman parameters remains to be done, but for one-loop applications, the integrals we need to know explicitly have maximally $N = 4$ external legs. Integrals with $N > 4$ can be expressed in terms

of boxes, triangles, bubbles and tadpoles (in the case of massive propagators). The analytic expressions for these “master integrals” are well-known. The most complicated analytic functions which can appear at one loop are dilogarithms.

The generic form of the derivation above makes clear that we do not have to go through the procedure of Wick rotation explicitly each time. All we need (for scalar integrals) is to use the following general formula for D -dimensional momentum integration (in Minkowski space, and after having performed the shift to have a quadratic form in the denominator):

$$\int \frac{d^D l}{i\pi^{\frac{D}{2}}} \frac{(l^2)^r}{[l^2 - R^2 + i\delta]^N} = (-1)^{N+r} \frac{\Gamma(r + \frac{D}{2})\Gamma(N - r - \frac{D}{2})}{\Gamma(\frac{D}{2})\Gamma(N)} [R^2 - i\delta]^{r-N+\frac{D}{2}} \quad (130)$$

Example one-loop two-point function

Applying the above procedure to our two-point function, we obtain

$$I_2 = \Gamma(2 - \frac{D}{2}) \int_0^1 dx [-p^2 x(1-x) + m^2 - i\delta]^{\frac{D}{2}-2}. \quad (131)$$

For $m^2 = 0$, the result can be expressed in terms of Γ -functions:

$$I_2 = (-p^2)^{\frac{D}{2}-2} \Gamma(2 - D/2) B(D/2 - 1, D/2 - 1), \quad (132)$$

where the $B(a, b)$ is defined in Eq. (128). The two-point function has an UV pole which is contained in

$$\Gamma(2 - D/2) = \Gamma(\epsilon) = \frac{1}{\epsilon} - \gamma_E + \mathcal{O}(\epsilon), \quad (133)$$

where γ_E is “Euler’s constant”, $\gamma_E = \lim_{n \rightarrow \infty} \left(\sum_{j=1}^n \frac{1}{j} - \ln n \right) = 0.5772156649 \dots$

Including the factor $g^2 \mu^{2\epsilon}$ which usually comes with the loop, and multiplying by $\frac{i\pi^{\frac{D}{2}}}{(2\pi)^D}$ for the normalisation conventions, we obtain

$$g^2 \mu^{2\epsilon} \frac{i\pi^{\frac{D}{2}}}{(2\pi)^D} I_2 = (4\pi)^\epsilon i \frac{g^2}{(4\pi)^2} \Gamma(\epsilon) (-p^2/\mu^2)^{-\epsilon} B(1 - \epsilon, 1 - \epsilon). \quad (134)$$

Remarks:

- As the combination $\Delta = \frac{1}{\epsilon} - \gamma_E + \ln(4\pi)$ always occurs in combination with a pole, in the so-called $\overline{\text{MS}}$ subtraction scheme (“modified Minimal Subtraction”), the whole combination Δ is subtracted in the renormalisation procedure.
- Scaleless integrals (i.e. integrals containing no dimensionful scale like masses or external momenta) are zero in dimensional regularisation, we use

$$\int_{-\infty}^{\infty} \frac{d^D k}{k^{2\rho}} = 0 . \quad (135)$$

Tensor integrals

If we have loop momenta in the numerator, the integration procedure is essentially the same, except for combinatorics and additional Feynman parameters in the numerator. The substitution $k = l - Q$ introduces terms of the form $(l - Q)^{\mu_1} \dots (l - Q)^{\mu_r}$ into the numerator of eq. (119). As the denominator is symmetric under $l \rightarrow -l$, only the terms with even numbers of l^μ in the numerator will give a non-vanishing contribution upon l -integration. We can use a *form factor representation* of a tensor integral, where the Lorentz structure has been extracted, each Lorentz tensor multiplying a scalar quantity, the *form factor*.

Historically, tensor integrals occurring in one-loop amplitudes were reduced to scalar integrals using so-called *Passarino-Veltman* reduction [54]. It is based on the fact that at one loop, scalar products of loop momenta with external momenta can always be expressed as combinations of propagators. The problem with Passarino-Veltman reduction is that it introduces powers of inverse Gram determinants $1/(\det G)^r$ for the reduction of a rank r tensor integral. This can lead to numerical instabilities upon phase space integration in kinematic regions where $\det G \rightarrow 0$.

Example for *Passarino-Veltman reduction*:

Consider the form factor representation of a rank one three-point integral

$$I_3^{D,\mu} = \int_{-\infty}^{\infty} d\kappa \frac{k^\mu}{[k^2 + i\delta][(k + p_1)^2 + i\delta][(k + p_1 + p_2)^2 + i\delta]} = A_1 r_1^\mu + A_2 r_2^\mu$$

$$r_1 = p_1 , r_2 = p_1 + p_2 .$$

Contracting with r_1 and r_2 and using the identities

$$k \cdot r_i = \frac{1}{2} [(k + r_i)^2 - k^2 - r_i^2] , i \in \{1, 2\}$$

we obtain, after cancellation of numerators

$$\begin{pmatrix} 2 r_1 \cdot r_1 & 2 r_1 \cdot r_2 \\ 2 r_2 \cdot r_1 & 2 r_2 \cdot r_2 \end{pmatrix} \begin{pmatrix} A_1 \\ A_2 \end{pmatrix} = \begin{pmatrix} R_1 \\ R_2 \end{pmatrix} \quad (136)$$

$$\begin{aligned} R_1 &= I_2^D(r_2) - I_2^D(r_2 - r_1) - r_1^2 I_3(r_1, r_2) \\ R_2 &= I_2^D(r_1) - I_2^D(r_2 - r_1) - r_2^2 I_3(r_1, r_2) . \end{aligned}$$

Solving for the form factors A_1 and A_2 we see that the solution involves the inverse of the Gram matrix $G_{ij} = 2 r_i \cdot r_j$.

Libraries where the scalar integrals and tensor one-loop form factors can be obtained numerically:

- `LoopTools` [55, 56]
- `OneLoop` [57]
- `golem95` [58–60]
- `Collier` [61]
- `Package-X` [62]

Scalar integrals only: `QCDLoop` [63, 64].

The calculation of one-loop amplitudes with many external legs is most efficiently done using “unitarity-cut-inspired” methods, for a review see e.g. Ref. [65]. One of the advantages is that it allows (numerical) reduction at *integrand level* (rather than integral level), which helps to avoid the generation of spurious terms which can blow up intermediate expressions.

4.5 Cancellation of infrared singularities

4.6 Parton evolution

5 Example: Higgs production

5.1 Higgs boson production in gluon fusion

5.2 Higgs boson pair production

5.3 Asymptotic expansions

References

- [1] ATLAS COLLABORATION collaboration, *Standard Model Summary Plots March 2021*, Tech. Rep. ATL-PHYS-PUB-2021-005, CERN, Geneva, Mar, 2021.
- [2] LHCb collaboration, R. Aaij et al., *Test of lepton universality in beauty-quark decays*, 2103.11769.
- [3] A. Crivellin, L. Hofer, J. Matias, U. Nierste, S. Pokorski and J. Rosiek, *Lepton-flavour violating B decays in generic Z' models*, *Phys. Rev. D* **92** (2015) 054013, [1504.07928].
- [4] MUON $g - 2$ COLLABORATION collaboration, e. a. Abi, B., *Measurement of the positive muon anomalous magnetic moment to 0.46 ppm*, *Phys. Rev. Lett.* **126** (Apr, 2021) 141801.
- [5] P. Athron, C. Balázs, D. H. Jacob, W. Kotlarski, D. Stöckinger and H. Stöckinger-Kim, *New physics explanations of a_μ in light of the FNAL muon $g - 2$ measurement*, 2104.03691.
- [6] ALEPH, DELPHI, L3, OPAL, SLD, LEP ELECTROWEAK WORKING GROUP, SLD ELECTROWEAK GROUP, SLD HEAVY FLAVOUR GROUP collaboration, S. Schael et al., *Precision electroweak measurements on the Z resonance*, *Phys. Rept.* **427** (2006) 257–454, [hep-ex/0509008].
- [7] T. C. Rogers, *An overview of transverse-momentum-dependent factorization and evolution*, *Eur. Phys. J. A* **52** (2016) 153, [1509.04766].
- [8] F. Dulat, A. Lazopoulos and B. Mistlberger, *iHixs 2 — Inclusive Higgs cross sections*, *Comput. Phys. Commun.* **233** (2018) 243–260, [1802.00827].
- [9] ATLAS collaboration, G. Aad et al., *Measurement of W^\pm and Z-boson production cross sections in pp collisions at $\sqrt{s} = 13$ TeV with the ATLAS detector*, *Phys. Lett. B* **759** (2016) 601–621, [1603.09222].

- [10] P. Skands, *Introduction to QCD*, in *Theoretical Advanced Study Institute in Elementary Particle Physics: Searching for New Physics at Small and Large Scales*, pp. 63–124, 2017. 1207.2389. DOI.
- [11] L. J. Dixon, *A brief introduction to modern amplitude methods*, in *Theoretical Advanced Study Institute in Elementary Particle Physics: Particle Physics: The Higgs Boson and Beyond*, pp. 31–67, 2014. 1310.5353. DOI.
- [12] V. Del Duca, L. J. Dixon and F. Maltoni, *New color decompositions for gauge amplitudes at tree and loop level*, *Nucl. Phys. B* **571** (2000) 51–70, [hep-ph/9910563].
- [13] Z. Bern and D. A. Kosower, *Color decomposition of one loop amplitudes in gauge theories*, *Nucl. Phys. B* **362** (1991) 389–448.
- [14] A. Gehrmann-De Ridder, T. Gehrmann, E. W. N. Glover, A. Huss and J. Pires, *Triple Differential Dijet Cross Section at the LHC*, *Phys. Rev. Lett.* **123** (2019) 102001, [1905.09047].
- [15] R. Abdul Khalek et al., *Phenomenology of NNLO jet production at the LHC and its impact on parton distributions*, *Eur. Phys. J. C* **80** (2020) 797, [2005.11327].
- [16] E. Laenen, *QCD*, in *Proceedings, 2014 European School of High-Energy Physics (ESHEP 2014): Garderen, The Netherlands, June 18 - July 01 2014*, pp. 1–58, 2016. 1708.00770.
- [17] R. V. Harlander and M. Steinhauser, *rhad: A Program for the evaluation of the hadronic R ratio in the perturbative regime of QCD*, *Comput. Phys. Commun.* **153** (2003) 244–274, [hep-ph/0212294].
- [18] <https://feynrules.irmp.ucl.ac.be/>.
- [19] Z. Trocsanyi, *QCD for collider experiments*, in *Proceedings, 2013 European School of High-Energy Physics (ESHEP 2013): Paradfurdo, Hungary, June 5-18, 2013*, pp. 65–116, 2015. 1608.02381. DOI.
- [20] D. Buttazzo, G. Degrassi, P. P. Giardino, G. F. Giudice, F. Sala, A. Salvio et al., *Investigating the near-criticality of the Higgs boson*, *JHEP* **12** (2013) 089, [1307.3536].

- [21] G. Heinrich, A. Maier, R. Nisius, J. Schlenk and J. Winter, *NLO QCD corrections to $W^+W^-b\bar{b}$ production with leptonic decays in the light of top quark mass and asymmetry measurements*, *JHEP* **06** (2014) 158, [1312.6659].
- [22] G. Heinrich, A. Maier, R. Nisius, J. Schlenk, M. Schulze, L. Scyboz et al., *NLO and off-shell effects in top quark mass determinations*, *JHEP* **07** (2018) 129, [1709.08615].
- [23] S. Dawson, C. Englert and T. Plehn, *Higgs Physics: It ain't over till it's over*, *Phys. Rept.* **816** (2019) 1–85, [1808.01324].
- [24] CMS collaboration, A. M. Sirunyan et al., *Measurements of $t\bar{t}H$ Production and the CP Structure of the Yukawa Interaction between the Higgs Boson and Top Quark in the Diphoton Decay Channel*, *Phys. Rev. Lett.* **125** (2020) 061801, [2003.10866].
- [25] ATLAS collaboration, G. Aad et al., *CP Properties of Higgs Boson Interactions with Top Quarks in the $t\bar{t}H$ and tH Processes Using $H \rightarrow \gamma\gamma$ with the ATLAS Detector*, *Phys. Rev. Lett.* **125** (2020) 061802, [2004.04545].
- [26] B. Grzadkowski, M. Iskrzynski, M. Misiak and J. Rosiek, *Dimension-Six Terms in the Standard Model Lagrangian*, *JHEP* **10** (2010) 085, [1008.4884].
- [27] F. Maltoni, E. Vryonidou and C. Zhang, *Higgs production in association with a top-antitop pair in the Standard Model Effective Field Theory at NLO in QCD*, *JHEP* **10** (2016) 123, [1607.05330].
- [28] J. Ellis, M. Madigan, K. Mimasu, V. Sanz and T. You, *Top, Higgs, Diboson and Electroweak Fit to the Standard Model Effective Field Theory*, 2012.02779.
- [29] P. A. Baikov, K. G. Chetyrkin, J. H. Kühn and J. Rittinger, *Complete $\mathcal{O}(\alpha_s^4)$ QCD Corrections to Hadronic Z-Decays*, *Phys. Rev. Lett.* **108** (2012) 222003, [1201.5804].
- [30] F. Herzog, B. Ruijl, T. Ueda, J. A. M. Vermaseren and A. Vogt, *On Higgs decays to hadrons and the R-ratio at N^4LO* , *JHEP* **08** (2017) 113, [1707.01044].

- [31] T. van Ritbergen, J. A. M. Vermaseren and S. A. Larin, *The Four loop beta function in quantum chromodynamics*, *Phys. Lett.* **B400** (1997) 379–384, [[hep-ph/9701390](#)].
- [32] P. A. Baikov, K. G. Chetyrkin and J. H. Kühn, *Five-Loop Running of the QCD coupling constant*, *Phys. Rev. Lett.* **118** (2017) 082002, [[1606.08659](#)].
- [33] F. Herzog, B. Ruijl, T. Ueda, J. A. M. Vermaseren and A. Vogt, *The five-loop beta function of Yang-Mills theory with fermions*, *JHEP* **02** (2017) 090, [[1701.01404](#)].
- [34] T. Luthe, A. Maier, P. Marquard and Y. Schröder, *The five-loop Beta function for a general gauge group and anomalous dimensions beyond Feynman gauge*, *JHEP* **10** (2017) 166, [[1709.07718](#)].
- [35] K. G. Chetyrkin, G. Falcioni, F. Herzog and J. A. M. Vermaseren, *Five-loop renormalisation of QCD in covariant gauges*, *JHEP* **10** (2017) 179, [[1709.08541](#)].
- [36] J. Davies, M. Steinhauser and D. Wellmann, *Completing the hadronic Higgs boson decay at order α_s^4* , *Nucl. Phys.* **B920** (2017) 20–31, [[1703.02988](#)].
- [37] D. J. Gross and F. Wilczek, *Ultraviolet Behavior of Nonabelian Gauge Theories*, *Phys. Rev. Lett.* **30** (1973) 1343–1346.
- [38] H. D. Politzer, *Reliable Perturbative Results for Strong Interactions?*, *Phys. Rev. Lett.* **30** (1973) 1346–1349.
- [39] P. A. Baikov, K. G. Chetyrkin and J. H. Kühn, *Quark Mass and Field Anomalous Dimensions to $\mathcal{O}(\alpha_s^5)$* , *JHEP* **10** (2014) 076, [[1402.6611](#)].
- [40] P. A. Baikov, K. G. Chetyrkin and J. H. Kühn, *Five-loop fermion anomalous dimension for a general gauge group from four-loop massless propagators*, *JHEP* **04** (2017) 119, [[1702.01458](#)].
- [41] A. G. Grozin, P. Marquard, A. V. Smirnov, V. A. Smirnov and M. Steinhauser, *Matching the heavy-quark fields in QCD and HQET at four loops*, *Phys. Rev. D* **102** (2020) 054008, [[2005.14047](#)].

- [42] F. Herren and A. E. Thomsen, *On Ambiguities and Divergences in Perturbative Renormalization Group Functions*, 2104.07037.
- [43] A. Gehrmann-De Ridder, T. Gehrmann, E. W. N. Glover and G. Heinrich, *NNLO corrections to event shapes in $e^+ e^-$ annihilation*, *JHEP* **12** (2007) 094, [0711.4711].
- [44] E. W. N. Glover, *Progress in NNLO calculations for scattering processes*, *Nucl. Phys. B Proc. Suppl.* **116** (2003) 3–7, [hep-ph/0211412].
- [45] J. Currie, E. W. N. Glover and J. Pires, *Next-to-Next-to Leading Order QCD Predictions for Single Jet Inclusive Production at the LHC*, *Phys. Rev. Lett.* **118** (2017) 072002, [1611.01460].
- [46] M. Czakon, A. van Hameren, A. Mitov and R. Poncelet, *Single-jet inclusive rates with exact color at $\mathcal{O}(\alpha_s^4)$* , *JHEP* **10** (2019) 262, [1907.12911].
- [47] B. Mistlberger, *Higgs boson production at hadron colliders at N^3LO in QCD*, *JHEP* **05** (2018) 028, [1802.00833].
- [48] C. Anastasiou, C. Duhr, F. Dulat, F. Herzog and B. Mistlberger, *Higgs Boson Gluon-Fusion Production in QCD at Three Loops*, *Phys. Rev. Lett.* **114** (2015) 212001, [1503.06056].
- [49] C. Duhr, F. Dulat, V. Hirschi and B. Mistlberger, *Higgs production in bottom quark fusion: matching the 4- and 5-flavour schemes to third order in the strong coupling*, *JHEP* **08** (2020) 017, [2004.04752].
- [50] C. Duhr, F. Dulat and B. Mistlberger, *Charged current Drell-Yan production at N^3LO* , *JHEP* **11** (2020) 143, [2007.13313].
- [51] J. Currie, A. Gehrmann-De Ridder, T. Gehrmann, E. W. N. Glover, A. Huss and J. a. Pires, *Infrared sensitivity of single jet inclusive production at hadron colliders*, *JHEP* **10** (2018) 155, [1807.03692].
- [52] G. 't Hooft and M. J. G. Veltman, *Regularization and Renormalization of Gauge Fields*, *Nucl. Phys.* **B44** (1972) 189–213.

- [53] C. G. Bollini and J. J. Giambiagi, *Dimensional Renormalization: The Number of Dimensions as a Regularizing Parameter*, *Nuovo Cim.* **B12** (1972) 20–26.
- [54] G. Passarino and M. J. G. Veltman, *One Loop Corrections for $e+ e-$ Annihilation Into $\mu+ \mu-$ in the Weinberg Model*, *Nucl. Phys.* **B160** (1979) 151–207.
- [55] T. Hahn, *Feynman Diagram Calculations with FeynArts, FormCalc, and LoopTools*, *PoS ACAT2010* (2010) 078, [1006.2231].
- [56] T. Hahn and M. Perez-Victoria, *Automatized one loop calculations in four-dimensions and D-dimensions*, *Comput. Phys. Commun.* **118** (1999) 153–165, [hep-ph/9807565].
- [57] A. van Hameren, *OneLOop: For the evaluation of one-loop scalar functions*, *Comput. Phys. Commun.* **182** (2011) 2427–2438, [1007.4716].
- [58] J. P. Guillet, G. Heinrich and J. F. von Soden-Fraunhofen, *Tools for NLO automation: extension of the golem95C integral library*, *Comput. Phys. Commun.* **185** (2014) 1828–1834, [1312.3887].
- [59] G. Cullen, J. P. Guillet, G. Heinrich, T. Kleinschmidt, E. Pilon, T. Reiter et al., *Golem95C: A library for one-loop integrals with complex masses*, *Comput. Phys. Commun.* **182** (2011) 2276–2284, [1101.5595].
- [60] T. Binoth, J. P. Guillet, G. Heinrich, E. Pilon and T. Reiter, *Golem95: A Numerical program to calculate one-loop tensor integrals with up to six external legs*, *Comput. Phys. Commun.* **180** (2009) 2317–2330, [0810.0992].
- [61] A. Denner, S. Dittmaier and L. Hofer, *Collier: a fortran-based Complex One-Loop Library in Extended Regularizations*, *Comput. Phys. Commun.* **212** (2017) 220–238, [1604.06792].
- [62] H. H. Patel, *Package-X: A Mathematica package for the analytic calculation of one-loop integrals*, *Comput. Phys. Commun.* **197** (2015) 276–290, [1503.01469].

- [63] S. Carrazza, R. K. Ellis and G. Zanderighi, *QCDLoop: a comprehensive framework for one-loop scalar integrals*, *Comput. Phys. Commun.* **209** (2016) 134–143, [1605.03181].
- [64] R. K. Ellis and G. Zanderighi, *Scalar one-loop integrals for QCD*, *JHEP* **02** (2008) 002, [0712.1851].
- [65] R. Ellis, Z. Kunszt, K. Melnikov and G. Zanderighi, *One-loop calculations in quantum field theory: from Feynman diagrams to unitarity cuts*, *Phys. Rept.* **518** (2012) 141–250, [1105.4319].